Electronic Supplementary Material (ESI) for CrystEngComm.
This journal is © The Royal Society of Chemistry 2023

Supporting Information

Structural and mechanistic studies of excitation- and temperature-tunable multicolor luminescence of triarylborane

Yangbin Xie,[a] Songshan Dai,[a] Yue Wang,[a] Xi Wang,[a] Ying Sun,[a] Zhenghua Ju,[a] Ran Fang,[b] Baoxin Zhang,*[,a] Jincai Wu,[a] Xiaoxiang Zhang, *[,c] Xiaobo Pan*[,a]

[a.] *State Key Laboratory of Applied Organic Chemistry (Lanzhou University), Key Laboratory of Nonferrous Metal Chemistry and Resources Utilization of Gansu Province, College of Chemistry and Chemical Engineering, Lanzhou University, Lanzhou 730000, People's Republic of China.*

[b.] *College of Chemistry and Chemical Engineering, Shaanxi University of Science and Technology, Xi'an 710021, People's Republic of China.*

[c.] *Lixiahe Agricultural Research Institute of Jiangsu Province, Yangzhou, Jiangsu 225007, China.*

Corresponding author:

E-mail: zhangbx@lzu.edu.cn, zhngyz@126.com, boxb@lzu.edu.cn.

General Information: Unless otherwise noted, all the chemicals were purchased from commercial sources and used without further purification. Dry THF was obtained through the distillation over sodium and benzophenone. The dimesityl(2-(phenylethynyl)phenyl)borane (**2**) was synthesized according to literature methods.[1] ^{1}H NMR, ^{13}C NMR and ^{11}B NMR were recorded in $CDCl_3$ on a JEOL JNM-ECS-400 MHz spectrometer. Tetramethylsilane was used as the internal standard. FT-IR spectra were carried out using a Bruker Vertex 70 at room temperature by using conventional KBr pellets method. UV-vis absorption spectra were recorded on a Lambda 950 recording spectrophotometer. Thermogravimetric analysis (TGA) was carried out in nitrogen atmosphere from 30 to 800 ºC with a ramping rate of 10 ºC min^{-1}. The CD spectra were recorded with OLIS DSM 1000. Powder X-Ray diffraction patterns were performed on an Rigaku D/Max-2400 X-ray diffractometer (XRD) with Cu Kα radiation (λ = 1.54184 Å) at 25 °C (scan range: 5−50°). Single crystal data was collected on a HyPix-6000HE CCD diffractometer using mirror monochromated Cu Kα radiation (λ = 1.54184 Å). Crystals structures were solved by direct methods using Olex 2−1.2. Subsequent difference Fourier analyses and least-squares refinement with SHELXL-2014/7 program package allowed for the location of the atom positions.[2-4]

The photoluminescence spectra, temperature dependent photoluminescence spectra and excitation spectra were measured on a Horiba FluoroMax-4 spectrofluorometer (Horiba Scientific). The lifetime and time-resolved emission spectra were measured on an Edinburgh FLS 920 combined fluorescence lifetime and steady state spectrometer equipped with a hydrogen lamp and a microsecond flash-lamp (μF920H), respectively. Mean decay times (τ_{ave}) were obtained from individual lifetimes τ_i and amplitudes a_i of multi-exponential evaluation. The total lifetimes of multi-sectioned PL-decay spectra are calculated using the following equation:

$$\tau_{ave} = \frac{\sum_{i=1}^{n} B_i \tau_i^2}{\sum_{i=1}^{n} B_i \tau_i}$$

$$\varphi_2 = \frac{B_2 \tau_2}{B_1 \tau_1 + B_2 \tau_2 + B_3 \tau_3} \cdot 100\%$$

where τ is the lifetime, i represents for the number of the lifetime components, and B_i is the proportion for each lifetime components, φ is percentage of the relative fluorescence intensity.

Experimental section

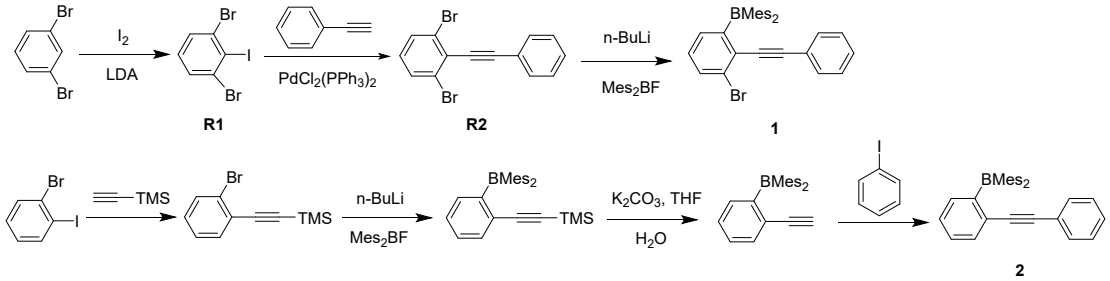

Scheme S1. Synthetic routes of compounds **1** and **2**.

Synthesis of (3-bromo-2-(phenylethynyl)phenyl)dimesitylborane (1): Compounds **R1** and **R2** were synthesized according to previously reported procedures.[5] Under argon, dissolve compound **R2** (1.01 g, 3.0 mmol) in freshly distilled THF (30 mL) solution in a 100 mL shrek reaction flask. Subsequently, ^{n}BuLi solution (2.25 mL, 3.6 mmol, 1.6 M in hexane) was added dropwise at -78 °C. After 3 hours at this temperature, Mes_2BF (0.97 g, 3.6 mmol) in tetrahydrofuran solution (15 mL) was added. The reaction was allowed slowly raised to room temperature after 1 hour and stirred overnight. After the reaction, it was quenched by adding saturated sodium chloride solution and extracted with dichloromethane (3 × 25 mL). The organic phases were combined, dried with anhydrous $MgSO_4$, and the solvent was distilled off under reduced pressure to obtain a yellow oily crude product. The residue was recrystallized from *n*-hexane to give compound **1** as light-yellow crystals at room temperature (0.92 g, 60.7 %). The crystals grown in *n*-hexane were dissolved in dichloromethane and the colorless block crystals were obtained from -25 ºC. ^{1}H NMR (400 MHz, $CDCl_3$, ppm, 293 K): δ 7.68 (d, J = 8.0 Hz, 1H), 7.22 (m, 4H), 7.11 (m, 3H), 6.77 (s, 4H), 2.26 (s, 6H), 2.02 (s, 12H); ^{13}C NMR (100 MHz, $CDCl_3$, ppm, 293 K): δ 140.96, 139.38, 134.14, 132.83, 131.70, 128.88, 128.47, 128.22, 127.88, 127.59, 123.16, 97.74, 88.66, 23.30, 21.31; ^{11}B NMR (128.3 MHz, $CDCl_3$, ppm, 293 K): δ 74.05. Anal. Calcd for $C_{32}H_{30}BBr$: C, 76.51; H, 5.72. Found: C, 76.06; H, 5.98.

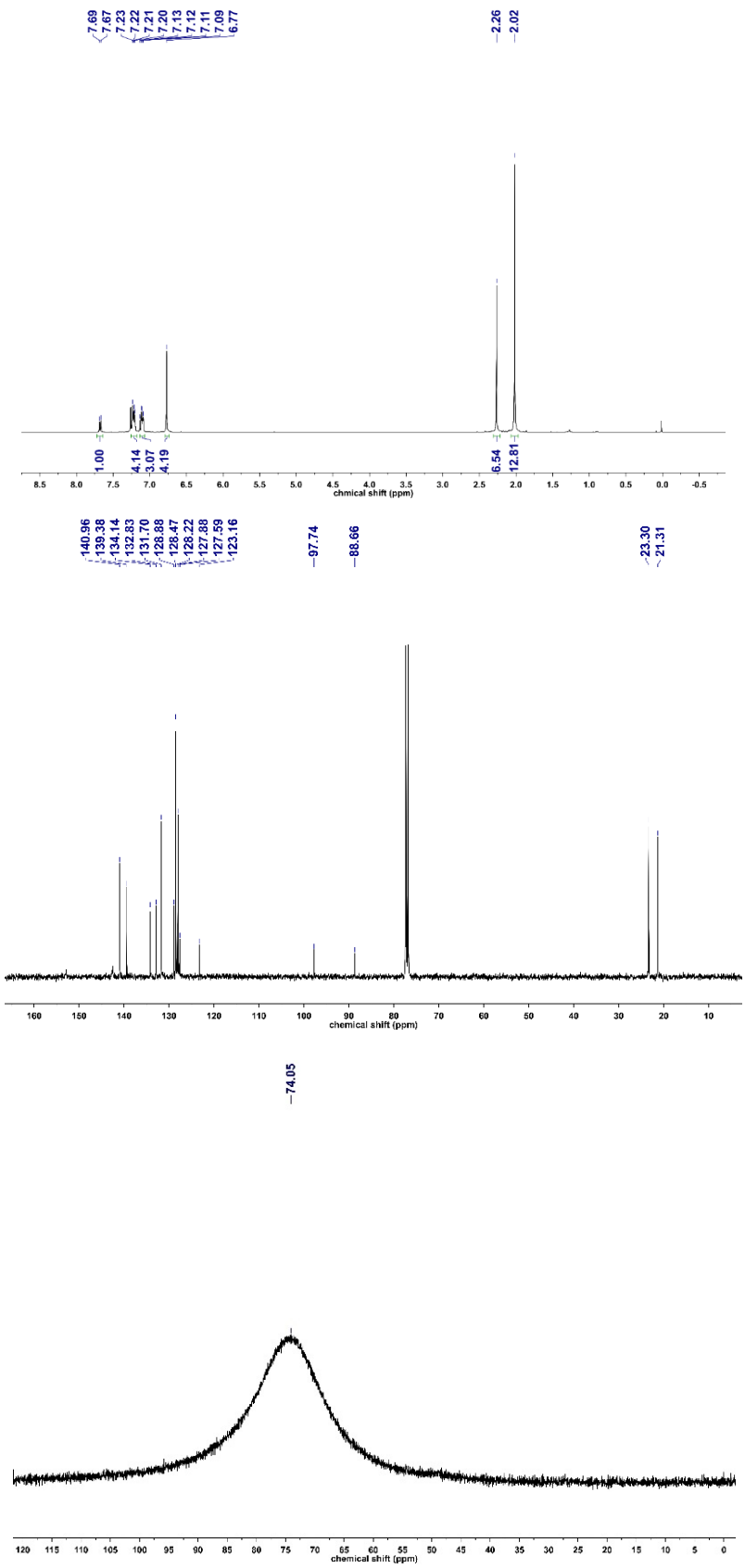

Figure S1. The ^{1}H (top, 400 MHz), ^{13}C (middle, 100 MHz), and ^{11}B (bottom, 128.3 MHz) NMR spectra of **1** were recorded in $CDCl_3$ at room temperature.

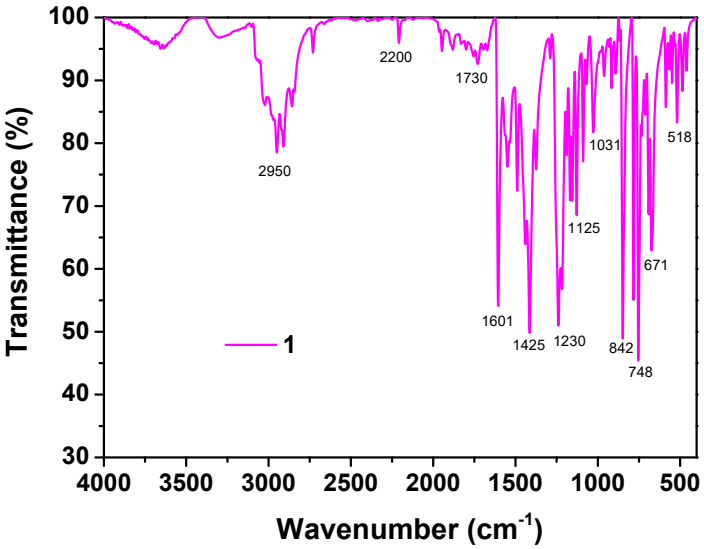

Figure S2. FT-IR spectrum of **1** at room temperature.

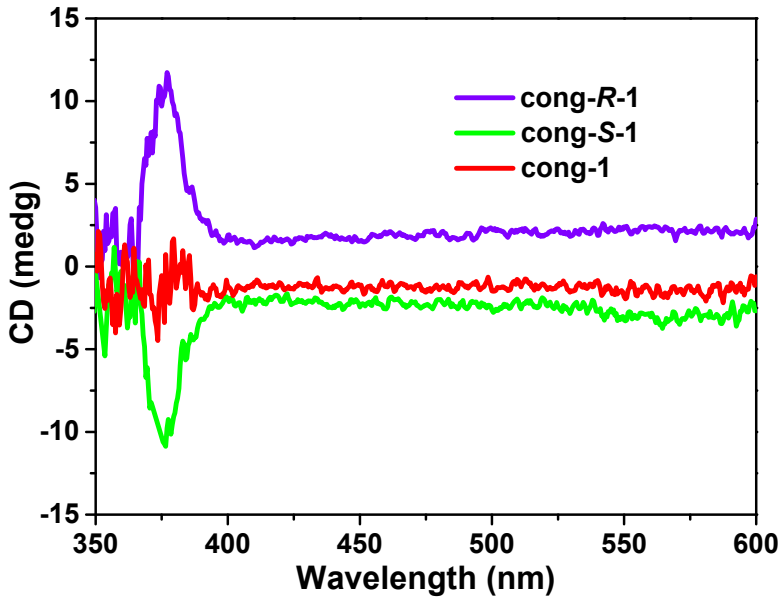

Figure S3. CD spectra of cong-*R*-**1**, cong-*S*-**1** and cong-**1** in film state.

Table S1. Single-crystal X-ray diffraction of **1**.

Identification code	rac-**1** -sunlight	rac-**1** -365nmUV	rac-**1** -395nmUV	cong-*R*-**1** -sunlight	cong-*R*-**1** -365nmUV	cong-*R*-**1** -395nmUV	cong-*S*-**1** -sunlight
Formula	$C_{32}H_{30}BBr$	$C_{32}H_{30}BBr$	$C_{32}H_{30}BBr$	$C_{32}H_{30}BBr$	$C_{32}H_{30}BBr$	$C_{32}H_{30}BBr$	$C_{32}H_{30}BBr$
Mr (g mol^{-1})	505.28	505.28	505.28	505.28	505.28	505.28	505.28
Crystal system	triclinic	triclinic	triclinic	orthorhombic	orthorhombic	orthorhombic	orthorhombic
Space group	P-1	P-1	P-1	$P2_12_12_1$	$P2_12_12_1$	$P2_12_12_1$	$P2_12_12_1$
T / K	275.5(3)	298.78(10)	298.86(10)	276.17(13)	276.85(13)	275.58(10)	299.50(18)
a (Å)	9.3313(3)	9.3292(5)	9.3353(5)	12.19552(12)	12.19617(12)	12.19480(12)	12.18719(19)
b (Å)	12.1551(3)	12.1601(4)	12.1678(4)	14.59669(15)	14.59644(14)	14.59820(14)	14.6021(2)
c (Å)	12.7667(3)	12.7627(5)	12.7548(6)	15.13390(14)	15.13369(15)	15.13607(15)	15.1221(2)
α (°)	71.773(2)	71.759(3)	71.785(4)	90	90	90	90
β (°)	81.625(2)	81.597(4)	81.609(4)	90	90	90	90
γ (°)	81.167(2)	81.225(4)	81.171(3)	90	90	90	90
V (Å^3)	1351.70(7)	1351.51(10)	1352.48(11)	2694.05(5)	2694.11(5)	2694.55(5)	2691.11(7)
Z	2	2	2	4	4	4	4
ρ_{calc} (g cm^{-3})	1.241	1.240	1.241	1.246	1.246	1.246	1.247
μ (mm^{-1})	2.181	2.181	2.179	2.188	2.188	2.188	2.191
F(000)	524	524	524	1048	1048	1048	1048
R_{int}	0.0403	0.0267	0.0302	0.0267	0.0257	0.0234	0.0261
GOF^c	1.039	1.023	1.041	1.048	1.058	1.056	1.112
$R_1{}^a$, $wR_2{}^b$ (I >2σ(I))	0.0501/0.1449	0.0445/0.1197	0.0457/0.1269	0.0321/0.0869	0.0309/0.0872	0.0304/0.0849	0.0377/0.1006
$R_1{}^a$, $wR_2{}^b$ (all date)	0.0584/0.1546	0.0514/0.1246	0.0532/0.1323	0.0338/0.0880	0.0326/0.0887	0.0320/0.0861	0.0394/0.1021
CCDC	2169199	2169197	2169196	2169201	2169195	2169198	2169200

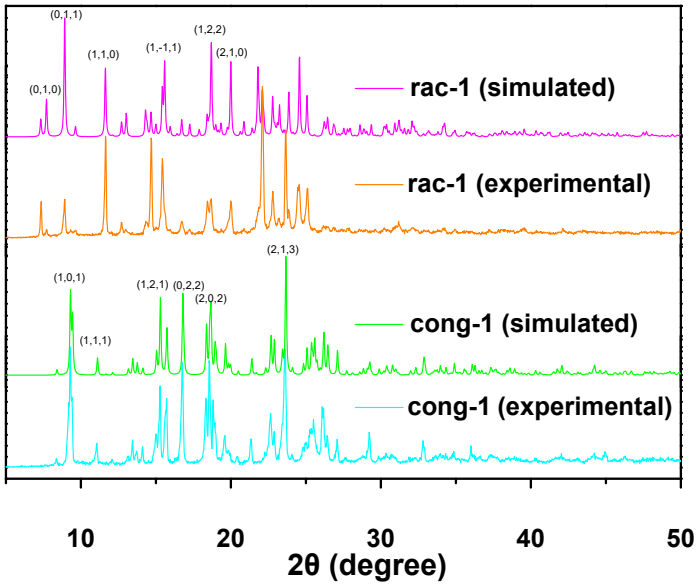

Figure S4. PXRD patterns of rac-**1** (from single crystal data: magenta; as-synthesis: orange) and cong-**1** (from single crystal data: green; as-synthesis: cyan).

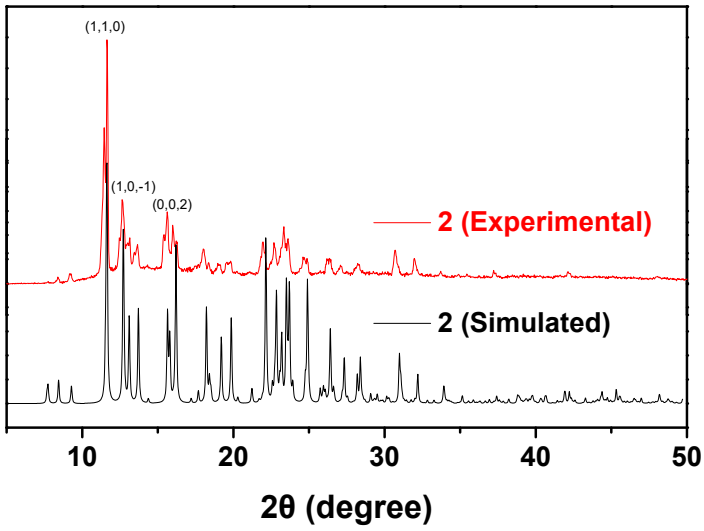

Figure S5. PXRD patterns of **2** (from single crystal data: pink; as-synthesis: violet).

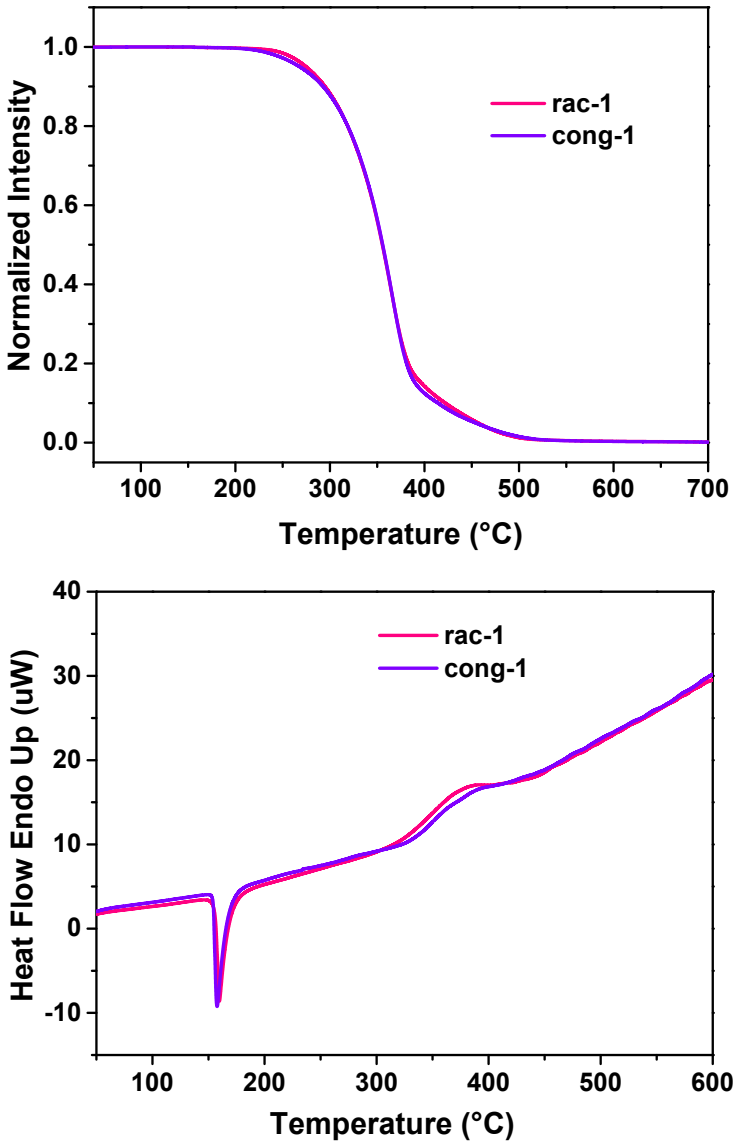

Figure S6. TGA curves and differential thermal analysis (DTA) analysis of rac-**1** and cong-**1**.

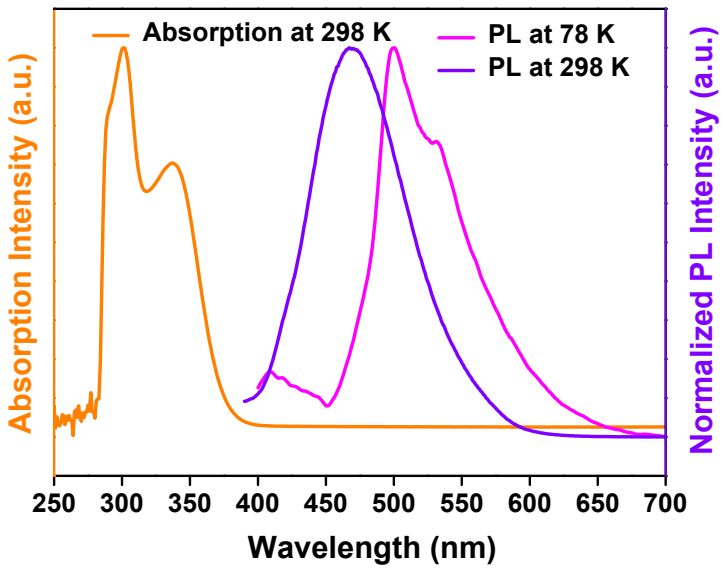

Figure S7. Normalized UV-vis absorption (orange line) and emission spectra (purple and magenta lines) of **1** in toluene (10 μM) solution under 78 and 298 K (λ_{ex} = 365 nm).

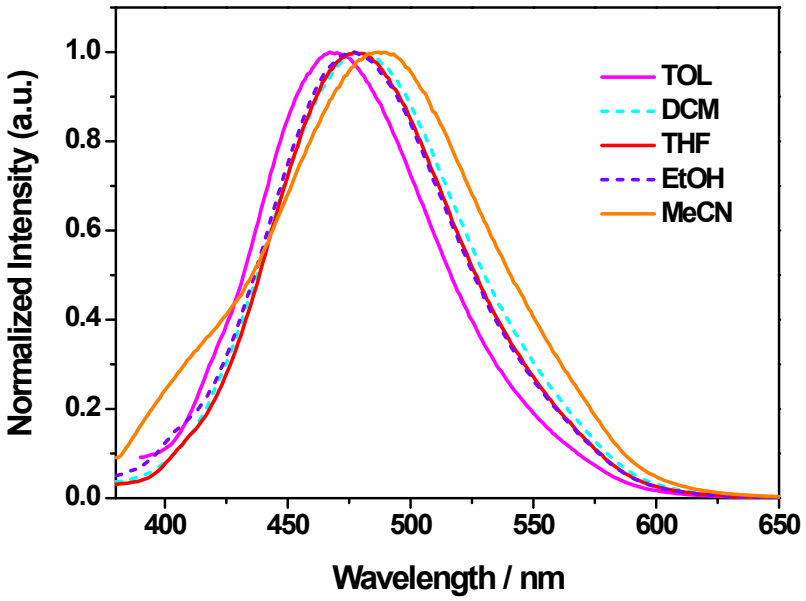

Figure S8. Normalized emission spectra of **1** in different polarities solvents (10 μM) under ambient conditions (λ_{ex} = 365 nm).

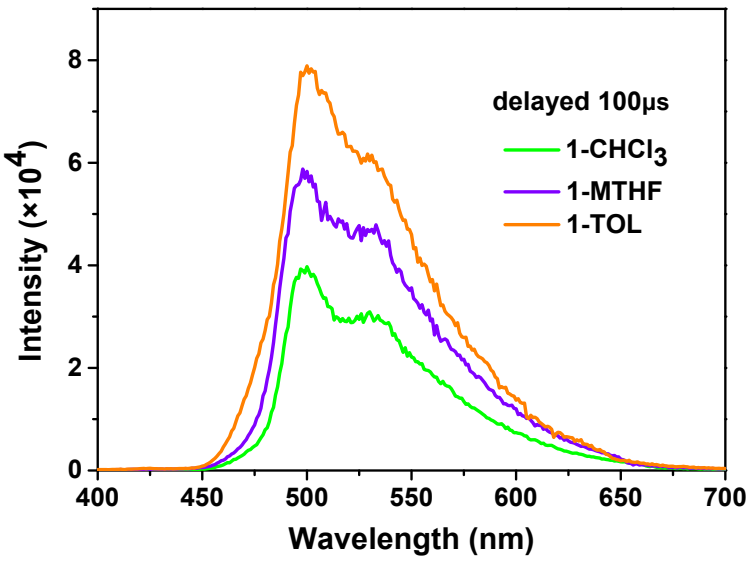

Figure S9. Transient PL spectra of **1** in various solvents (10 μM) at 78 K (delayed 100 μs, λ_{ex} = 365 nm).

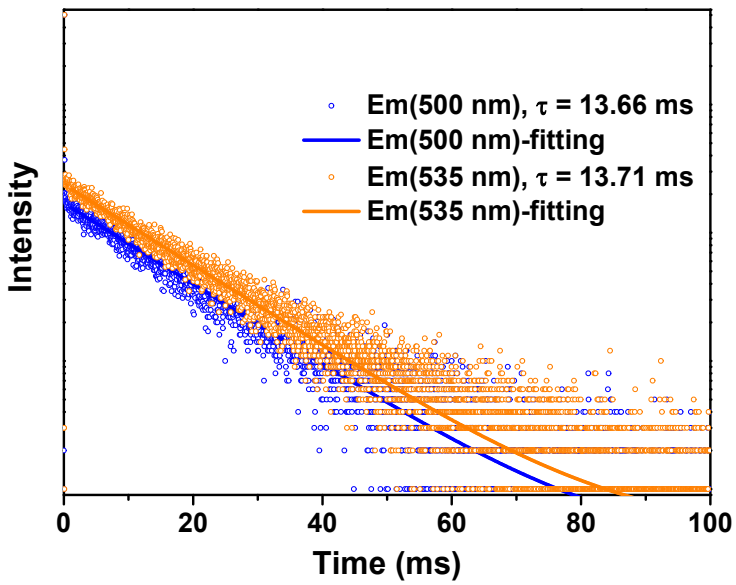

Figure S10. Transient PL decay curves of **1** in toluene solution (20.0 μM) at 78 K (λ_{ex} = 365 nm).

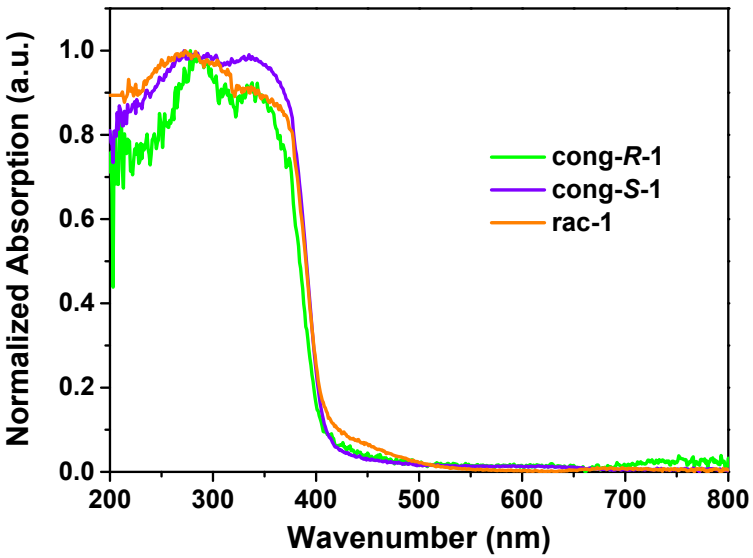

Figure S11. Normalized absorption spectra of the **1** crystals in each form.

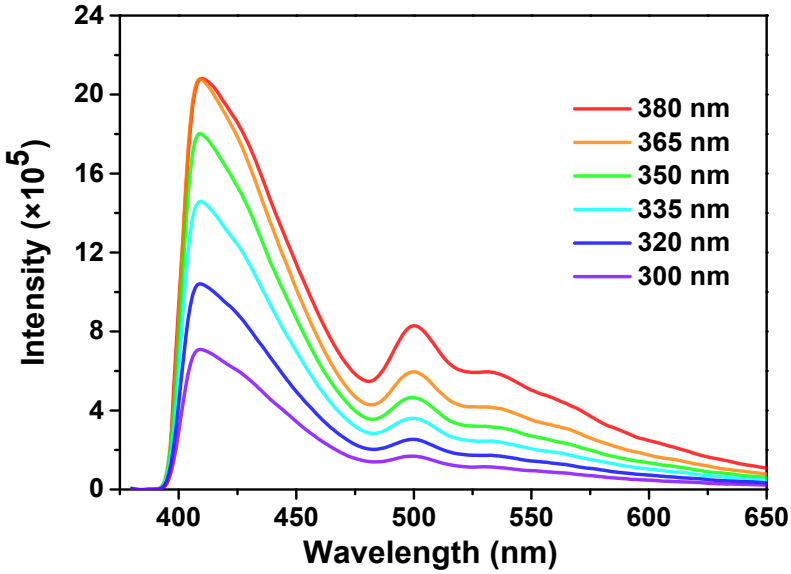

Figure S12. Excitation-wavelength-tunable steady-state emission spectra of rac-**1** in powder.

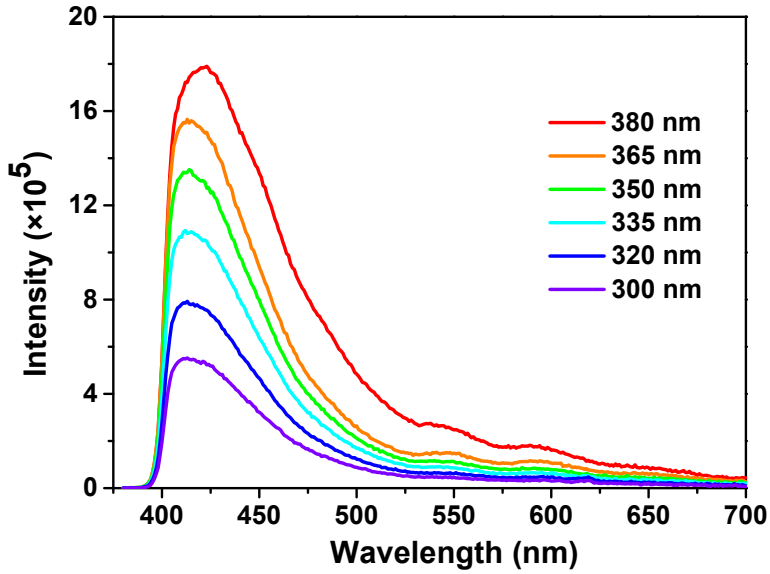

Figure S13. Excitation-wavelength-tunable steady-state emission spectra of cong-**1** in powder.

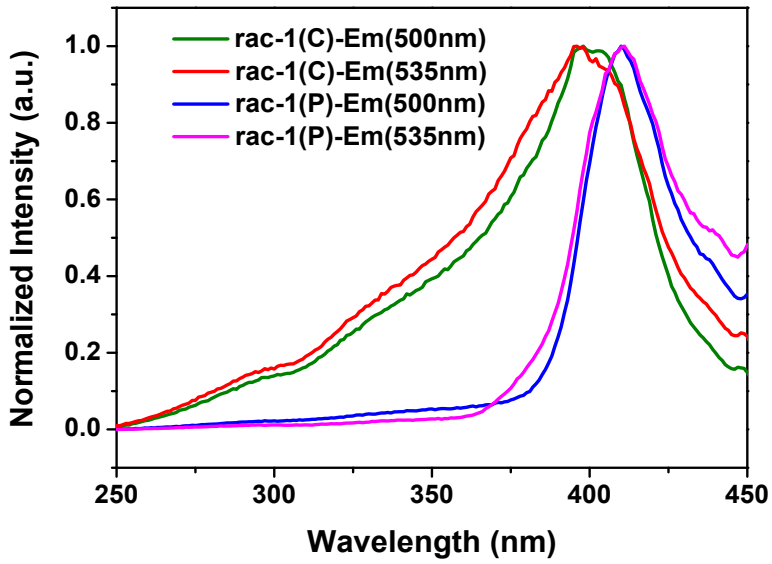

Figure S14. The corresponding excitation spectra of the different emission peaks of rac-**1** in crystals (C) and powder (P) at 500 and 535 nm, respectively.

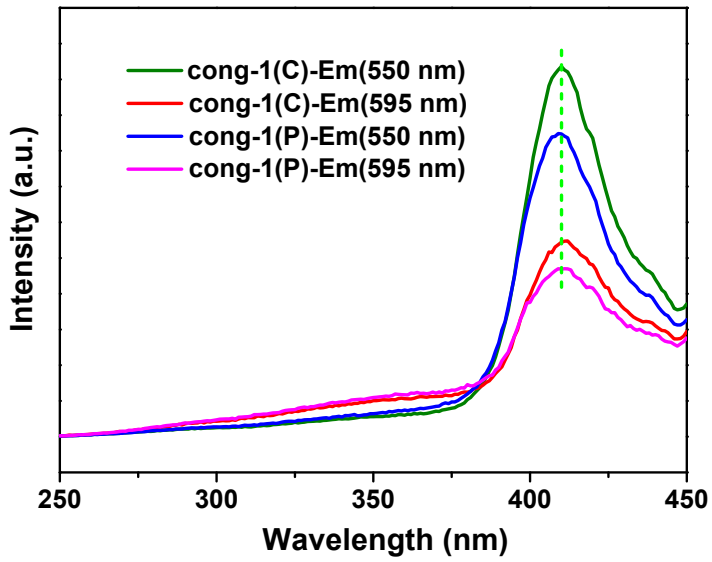

Figure S15. The corresponding excitation spectra of the different emission peaks of cong-**1** in crystals (C) and powder (P) at 550 and 595 nm, respectively.

Table S2. Lifetimes (τ) of rac-**1** at different excitation wavelengths in crystals (C) and powder (P), respectively (λ_{em} = 415 nm).

Sample	Excitation wavelength/nm	Fluorescence				
		τ_F/ns	B_i	Rel.%	τ_{ave}/ns	χ^2
rac-**1** (C)	300	0.24 4.17	1.11 0.004	94.46 5.54	0.47	1.073
	320	0.22 5.64	1.11 0.001	97.32 2.68	0.34	1.029
	335	0.26 5.29	0.10 0.0001	97.24 2.76	0.37	1.030
	350	0.23 5.13	0.11 0.0001	97.54 2.46	0.33	1.072
	365	0.25 6.24	0.10 0.00008	98.09 1.91	0.36	1.001
	380	0.23 1.87 8.69	0.11 0.001 0.0001	88.86 5.60 5.55	0.62	1.016
rac-**1** (P)	300	0.27 2.95	0.10 0.0002	97.49 2.51	0.33	1.006
	320	0.20 5.14	0.13 0.00006	98.87 1.13	0.26	1.004
	335	0.19 4.60	0.12 0.00005	99.01 0.99	0.23	1.004
	350	0.24 4.74	0.11 0.00008	98.62 1.38	0.31	1.017
	365	0.25 5.08	0.10 0.00006	98.85 1.15	0.31	1.036
	380	0.19 7.10	0.13 0.0001	96.71 3.29	0.38	1.018

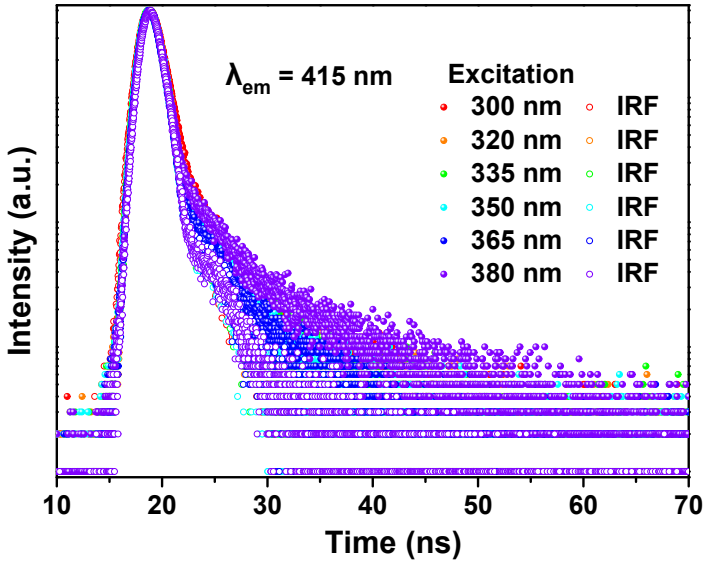

Figure S16. PL decay curves of rac-**1** crystals measured at different excitation wavelengths (λ_{em} = 415 nm).

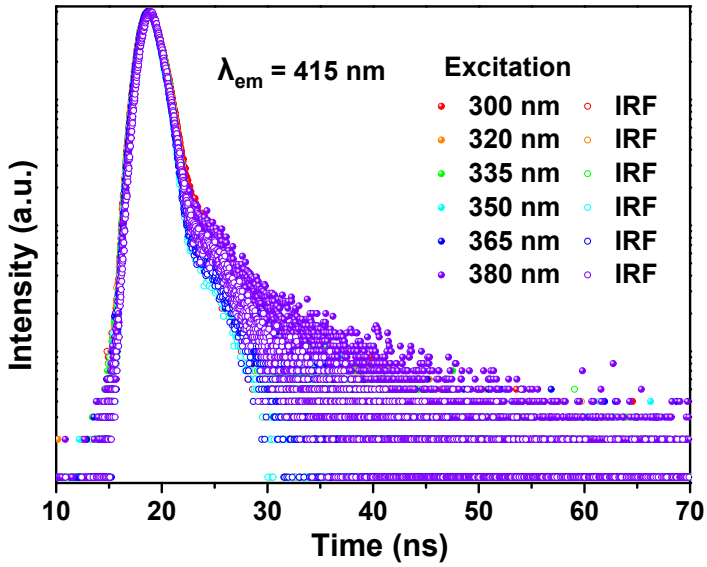

Figure S17. PL decay curves of rac-**1** powder measured at different excitation wavelengths (λ_{em} = 415 nm).

Table S3. Lifetimes (τ) of cong-**1** at different excitation wavelengths in crystals (C, 427 nm) and powder (P, 424 nm), respectively.

Sample	Excitation wavelength/nm	Fluorescence				
		τ_F/ns	B_i	Rel.%	τ_{ave}/ns	χ^2
cong-**1** (C)	300	0.22 1.10 7.26	0.10 0.004 0.0002	78.32 17.29 4.39	0.73	1.001
	320	0.20 6.48	0.12 0.0001	96.25 3.75	0.36	1.017
	335	0.28 6.84	0.09 0.0001	96.94 3.06	0.45	1.074
	350	0.28 7.73	0.09 0.00009	97.47 2.53	0.48	1.079
	365	0.28 7.58	0.09 0.0001	96.15 3.85	0.49	1.062
	380	0.27 1.49 8.94	0.08 0.003 0.0003	75.56 12.57 11.87	1.24	1.030
cong-**1** (P)	300	0.28 1.08 6.92	0.01 0.002 0.004	91.52 7.02 1.45	6.04	1.006
	320	0.21 7.12	0.12 0.00005	98.62 1.38	0.31	1.055
	335	0.18 6.59	0.14 0.00005	98.60 1.40	0.26	1.027
	350	0.18 8.05	0.13 0.00004	98.54 1.46	0.28	0.998
	365	0.27 7.04	0.10 0.0001	97.11 2.89	0.45	1.009
	380	0.26 1.16 8.23	0.09 0.003 0.0003	80.08 10.16 9.76	1.04	1.089

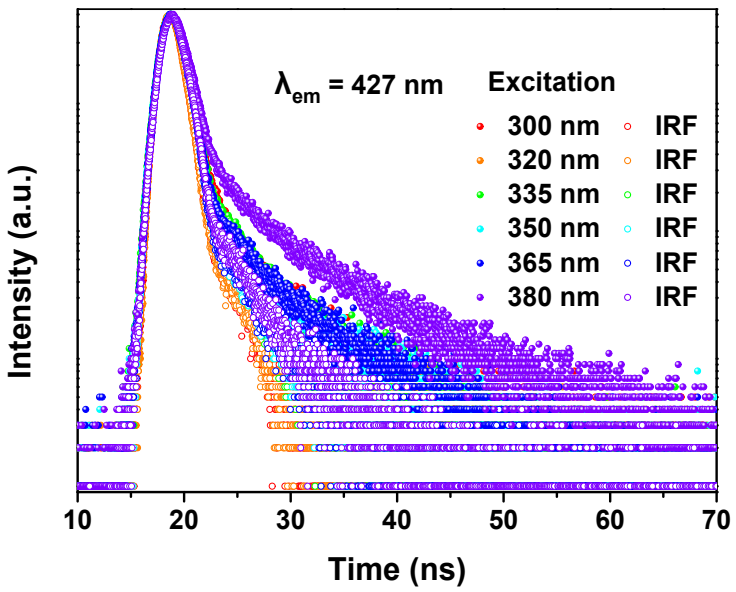

Figure S18. PL decay curves of cong-**1** crystals measured at different excitation wavelengths (λ_{em} = 427 nm).

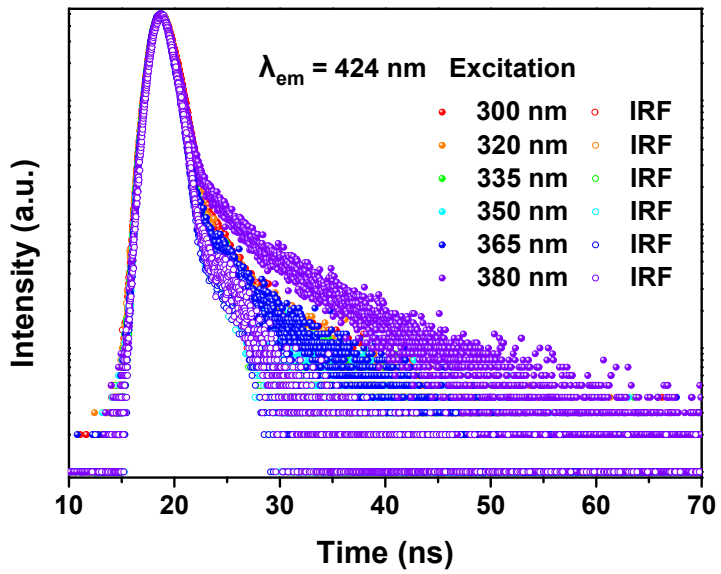

Figure S19. PL decay curves of cong-**1** crystals measured at different excitation wavelengths (λ_{em} = 424 nm).

Table S4. Photoluminescence lifetimes (τ) of rac-**1** at different excitation wavelengths at 500 and 535 nm, respectively.

Sample	Excitation wavelength/nm	λ_{em}/nm	τ_p/μs	χ^2	λ_{em}/nm	τ_p/μs	χ^2
rac-**1** (C)	300	500	174.91	1.012	535	180.34	1.041
	320		183.21	1.017		186.19	1.048
	335		183.42	1.002		189.57	1.018
	350		207.16	1.053		219.43	1.028
	365		293.61	1.064		307.98	1.079
	380		374.32	1.051		395.20	1.054
rac-**1** (P)	300	500	81.14	1.112	535	83.21	1.054
	320		81.19	1.084		83.91	1.052
	335		85.07	1.085		84.00	1.017
	350		85.39	1.054		93.75	1.064
	365		107.01	1.029		104.73	1.082
	380		133.49	1.047		145.33	1.019

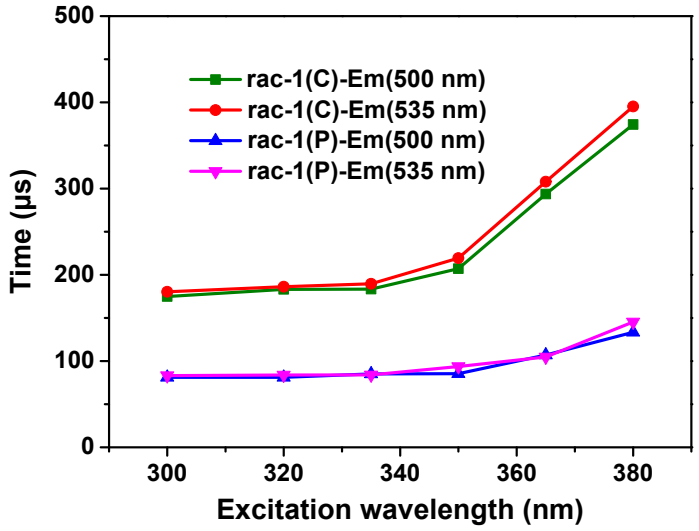

Figure S20. The trend of rac-**1** lifetimes in crystals and powder at different excitation wavelengths at 500 and 535 nm.

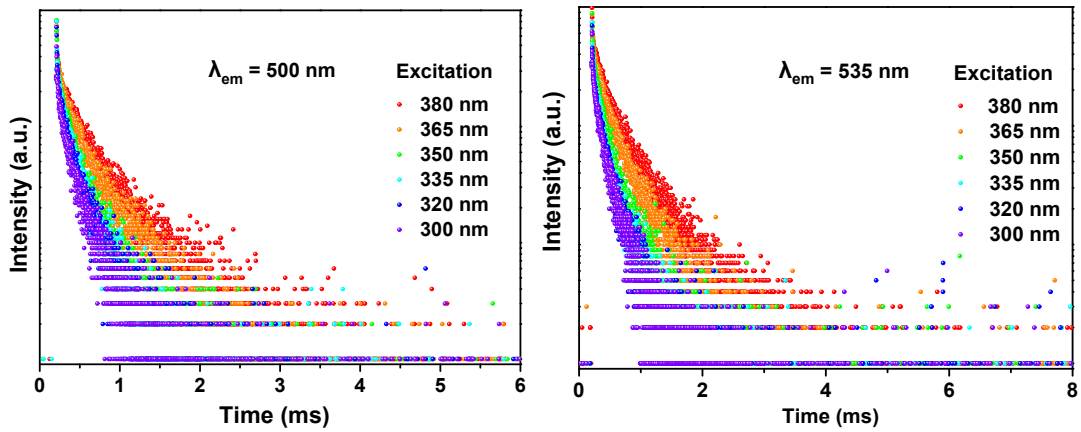

Figure S21. PL decay curves of rac-**1** crystals measured at 500 and 535 nm at different excitation wavelengths.

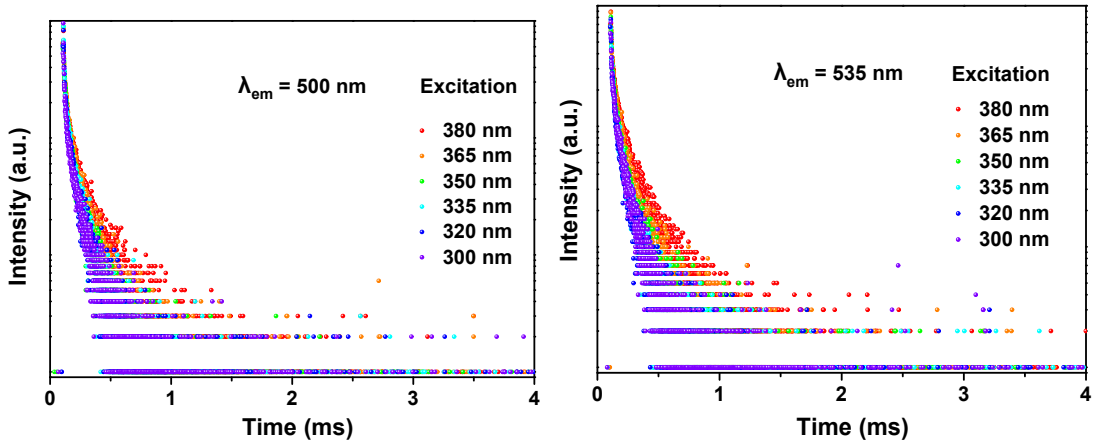

Figure S22. PL decay curves of rac-**1** powder measured at 500 and 535 nm at different excitation wavelengths.

Table S5. Photoluminescence lifetimes (τ) of cong-**1** at different excitation wavelengths at 550 and 595 nm, respectively.

Sample	Excitation wavelength/nm	λ_{em}/nm	τ_p/μs	χ^2	λ_{em}/nm	τ_p/μs	χ^2
cong-**1** (C)	300	550	155.89	1.005	595	536.82	1.004
	320		216.40	1.008		660.82	1.007
	335		509.95	1.004		669.73	1.035
	350		593.60	1.072		674.81	1.002
	365		683.79	1.001		696.55	1.005
	380		733.67	1.001		774.26	1.000
cong-**1** (P)	300	550	133.20	1.032	595	169.35	1.034
	320		143.82	1.014		176.73	1.003
	335		494.75	1.020		396.14	1.024
	350		524.68	1.019		404.69	1.001
	365		596.06	1.019		542.64	1.004
	380		721.02	1.017		637.67	1.004

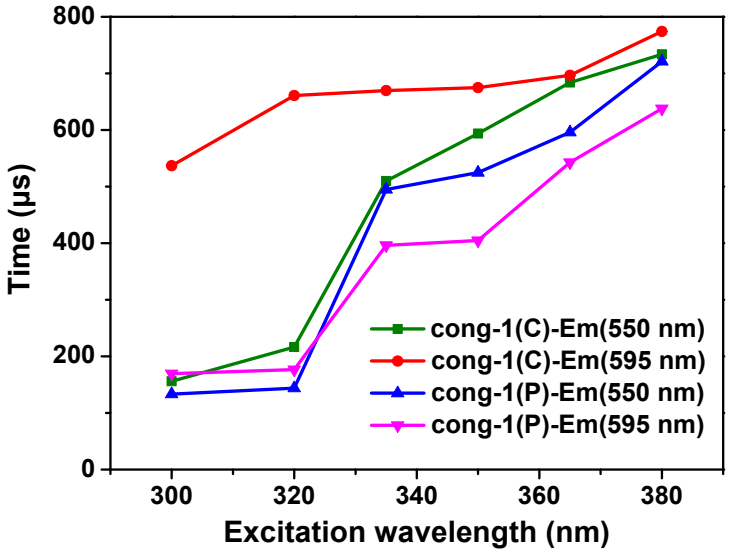

Figure S23. The trend of cong-**1** lifetimes in crystals and powder at different excitation wavelengths at 550 and 595 nm.

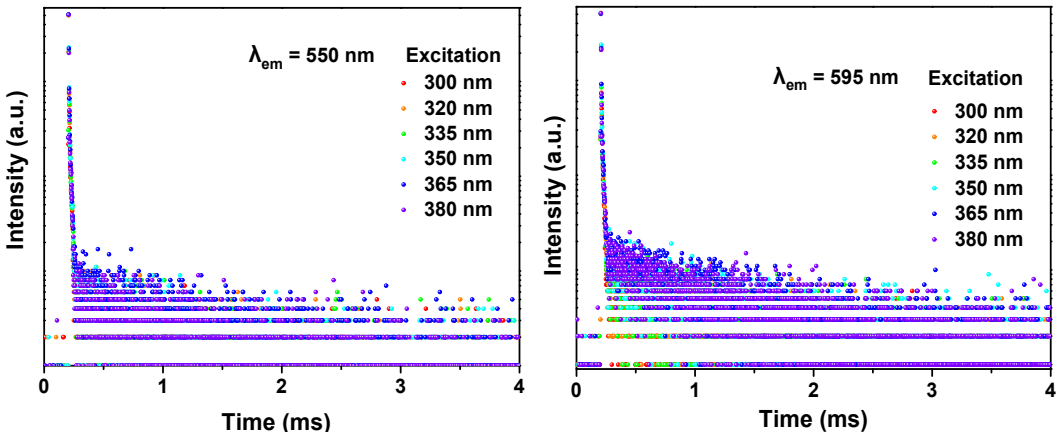

Figure S24. PL decay curves of cong-**1** crystal measured at 550 and 595 nm at different excitation wavelengths.

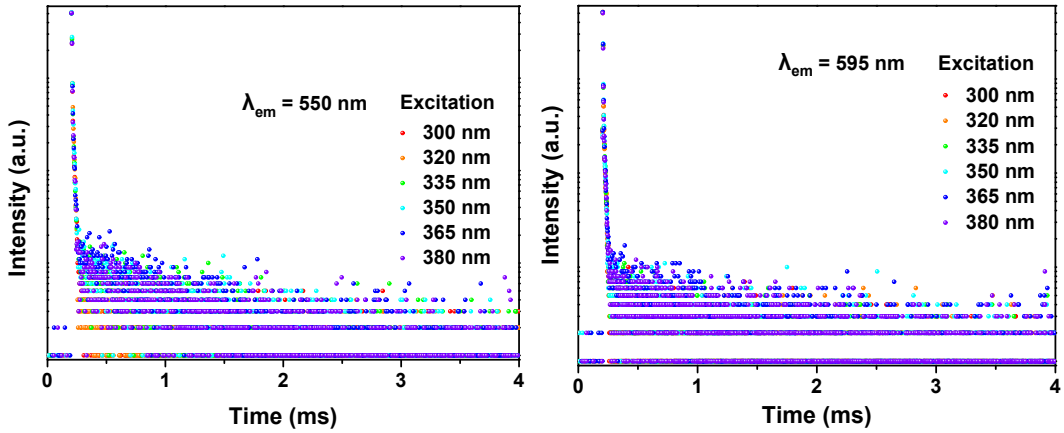

Figure S25. PL decay curves of cong-**1** powder measured at 550 and 595 nm at different excitation wavelengths.

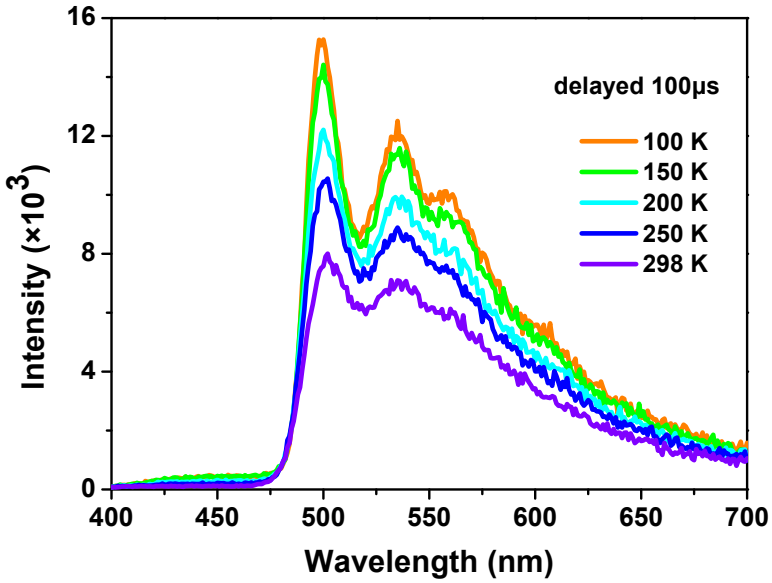

Figure S26. Steady-state and transient PL spectra of rac-**1** crystal at different temperatures (delayed 100 μs, λ_{ex} = 365 nm).

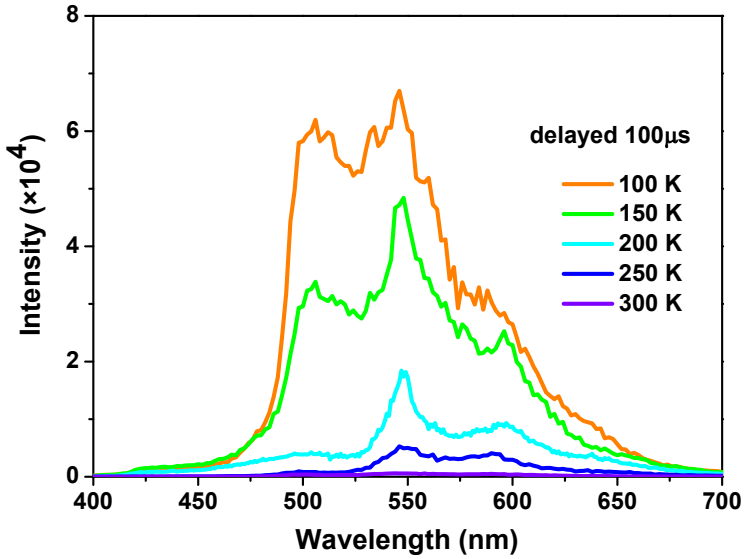

Figure S27. Steady-state and transient PL spectra of cong-**1** crystal at different temperatures (delayed 100 μs, λ_{ex} = 365 nm).

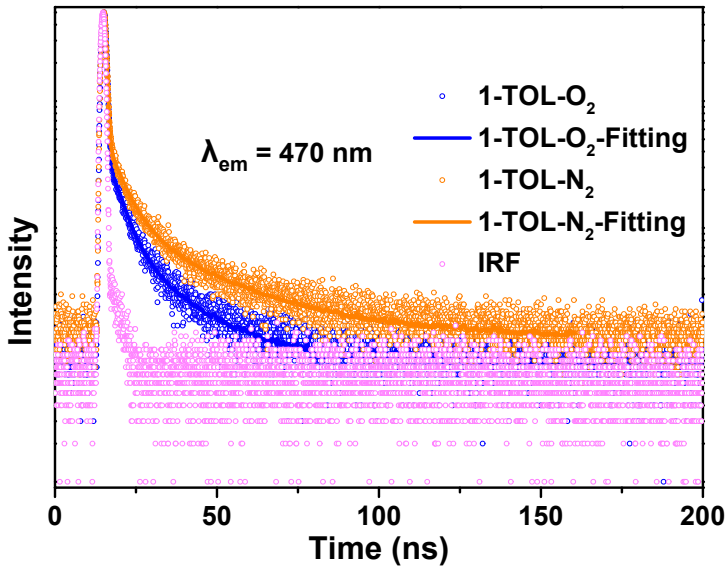

Figure S28. Transient PL decay curves of **1** in toluene solution (20.0 μM) bubbling nitrogen/oxygen (λ_{ex} = 365 nm).

Table S6. The lifetimes (τ) of **1** in toluene solution (20.0 μM) bubbling nitrogen/oxygen, respectively.

Parameters	**N_2**	**O_2**
τ_1(ns)	0.41	0.36
B_1	0.14	0.15
Rel. %	65.12	75.80
τ_2(ns)	5.58	4.52
B_2	0.003	0.002
Rel. %	16.35	13.36
τ_3(ns)	27.47	17.82
B_3	0.001	0.0004
Rel. %	18.53	10.84
χ^2	1.069	1.106
τ_{avg}(ns)	8.64	2.65

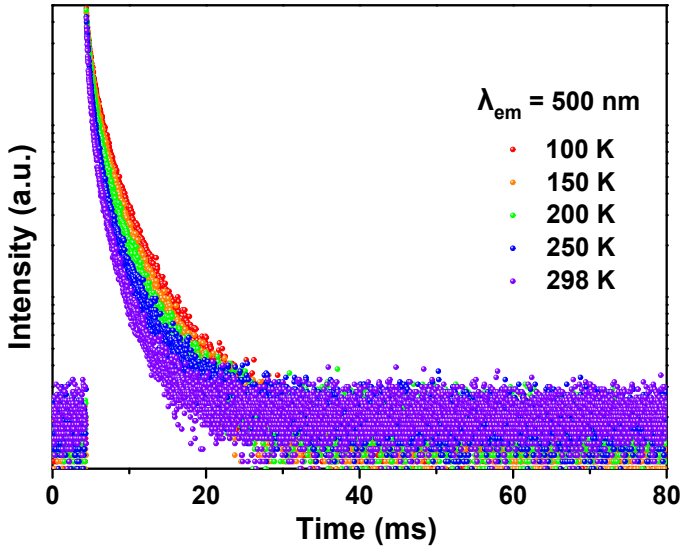

Figure S29. Transient PL decay curves of rac-**1** crystal measured at 500 nm at different temperatures (λ_{ex} = 365 nm).

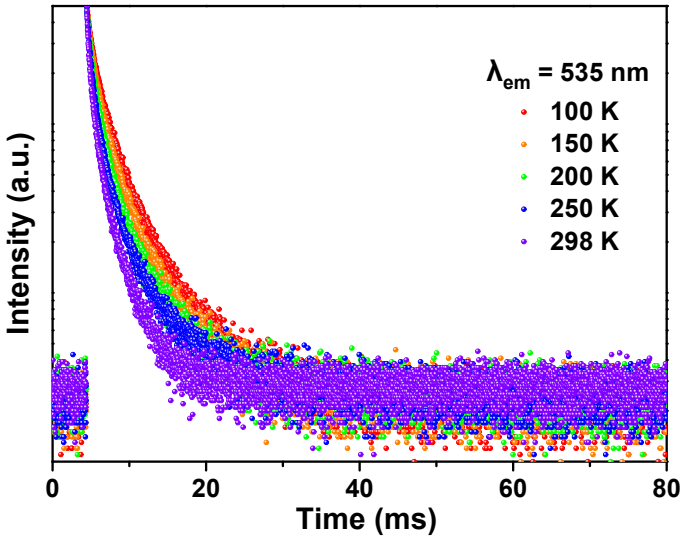

Figure S30. Transient PL decay curves of rac-**1** crystal measured at 535 nm at different temperatures (λ_{ex} = 365 nm).

Table S7. The lifetime of rac-**1** crystal measured at 550 and 595 nm at different temperatures (λ_{ex} = 365 nm).

rac-1	T/K	A_1	τ_1/ms	A_2	τ_2/ms	χ^2	τ_{avg}/ms
500 nm	100	2.05	2.94	3.18	0.55	0.998	2.40
	150	1.86	2.74	3.05	0.57	0.998	2.19
	200	3.53	0.49	1.78	2.44	0.998	1.89
	250	3.84	0.41	1.38	2.24	0.998	1.62
	298	1.39	1.75	4.59	0.29	0.998	1.24
535 nm	100	3.43	0.61	2.61	3.11	0.999	2.60
	150	2.29	2.86	3.68	0.60	0.999	2.29
	200	2.13	2.45	4.35	0.49	0.998	1.88
	250	1.90	2.24	5.37	0.41	0.998	1.62
	298	1.92	1.64	5.09	0.27	0.998	1.22

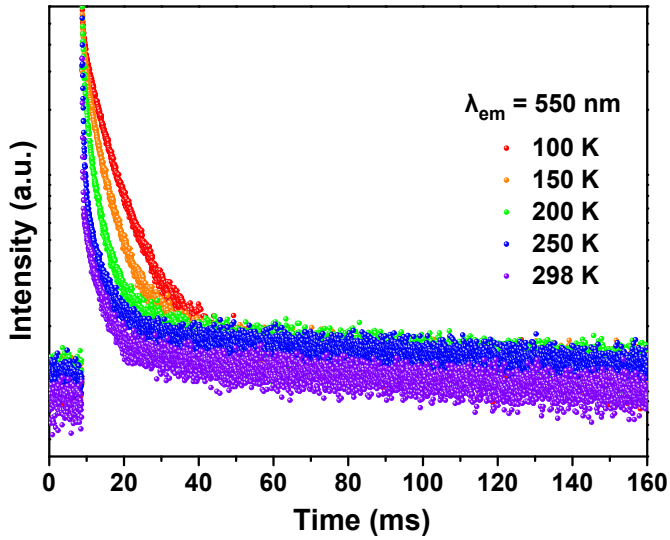

Figure S31. PL decay curves of cong-**1** crystal measured at 550 nm at different temperatures (λ_{ex} = 365 nm).

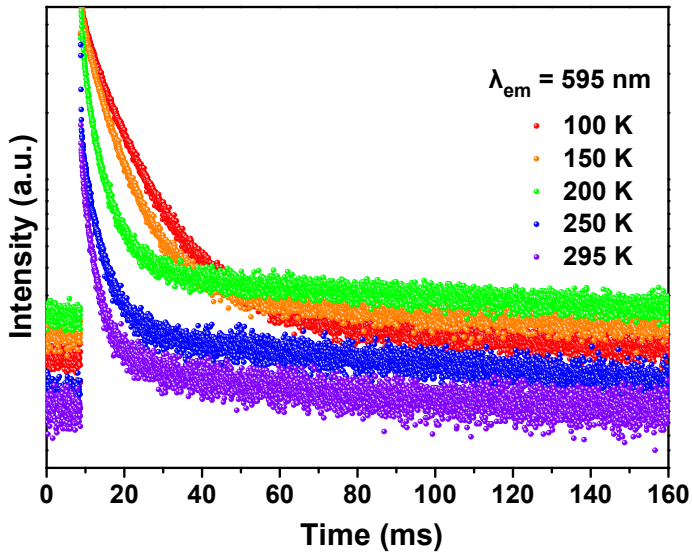

Figure S32. PL decay curves of cong-**1** crystal measured at 595 nm at different temperatures (λ_{ex} = 365 nm).

Table S8. The lifetime of cong-**1** crystals measured at 550 and 595 nm at different temperatures (λ_{ex} = 365 nm).

cong-1	T/K	A_1	τ_1/ms	A_2	τ_2/ms	χ^2	τ_{avg}/ms
550 nm	100	3.86	5.88	2.37	0.40	0.998	5.66
	150	3.45	4.26	2.86	0.40	0.997	3.98
	200	2.49	3.05	5.07	0.36	0.997	2.53
	250	0.92	0.58	0.55	4.56	0.992	3.86
	298	1.88	0.13	0.54	3.73	0.987	3.35
595 nm	100	4.69	8.37	1.02	1.03	0.999	8.18
	150	1.41	0.89	4.63	6.50	0.999	6.27
	200	3.58	0.62	3.09	3.95	0.998	3.44
	250	1.37	3.44	9.68	0.07	0.994	2.99
	298	0.98	2.90	0.80	0.35	0.992	2.67

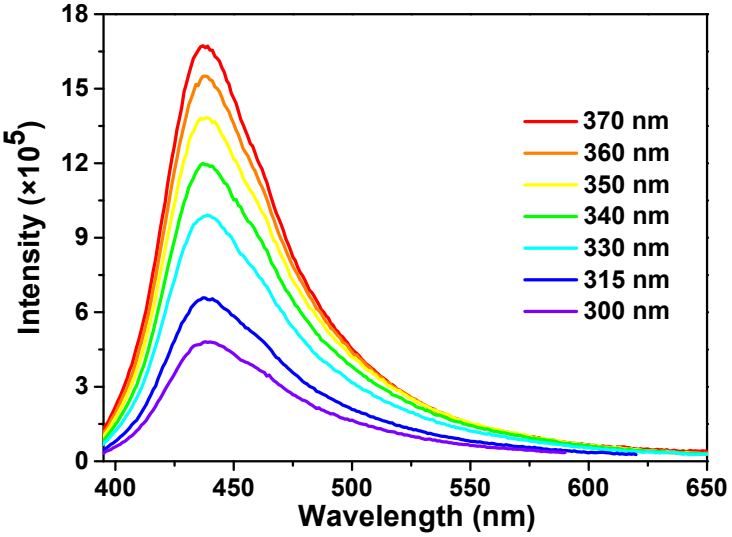

Figure S33. Excitation-wavelength-tunable steady-state PL spectra of **2** in crystals.

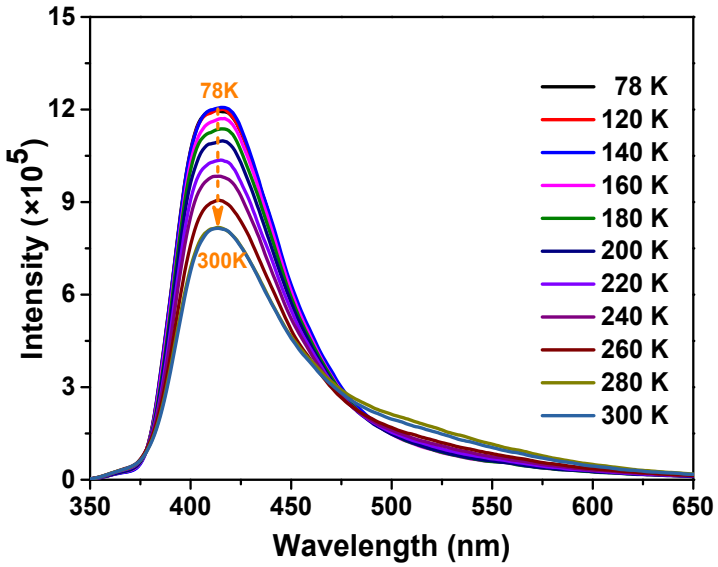

Figure S34. Steady-state PL spectra measured at different temperatures of compound **2** (from 78 to 300 K, λ_{ex} = 330 nm).

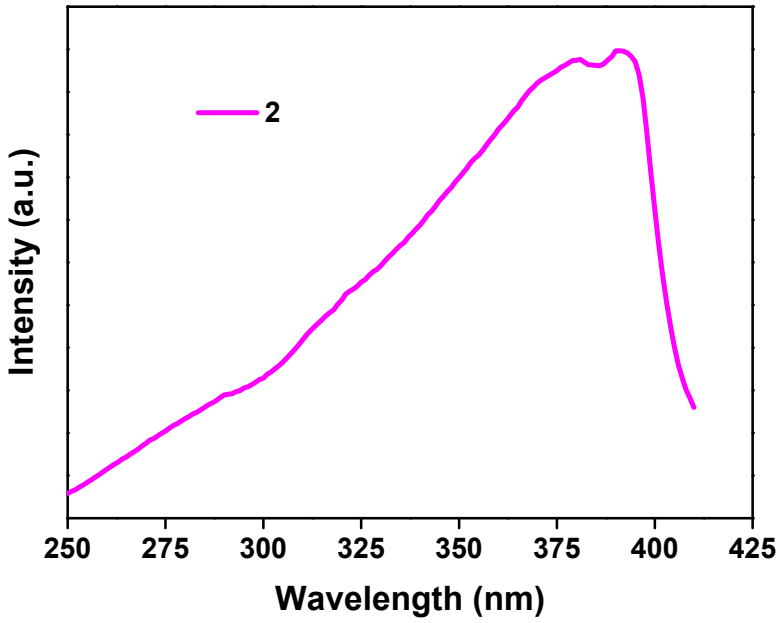

Figure S35. The excitation spectrum of compound **2** in crystals at 437 nm.

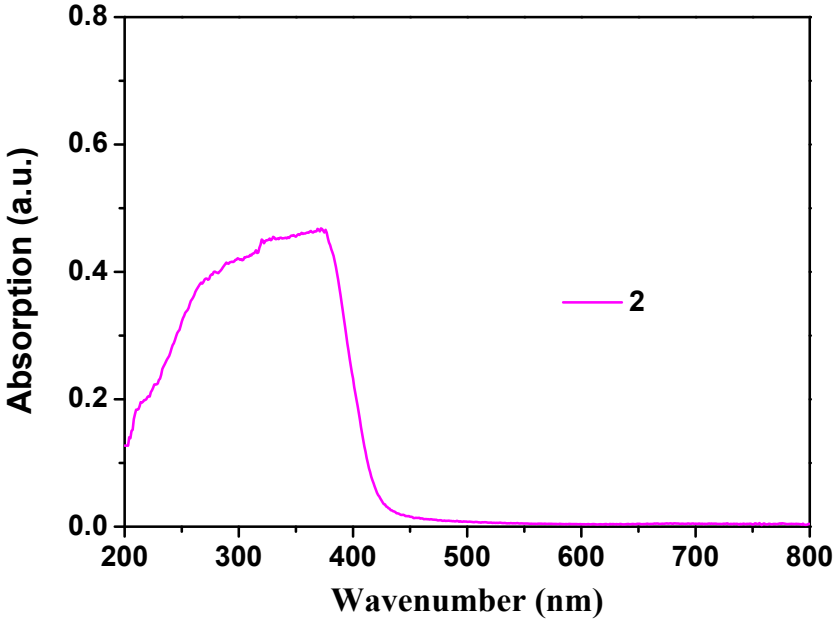

Figure S36. The UV-vis spectrum of compound **2**.

Table S9. Selected dihedral angle, intramolecular C-H···π and intermolecular C-H···Br of rac-**1** and cong-*R*-**1** at sunlight.

Dihedral angle (°)				
Parameter		Sunlight	UV 365	UV 395
P1-P2	rac-**1**	10.97(13)	10.84(12)	11.04(13)
	cong-*R*-**1**	44.18(14)	43.97(14)	44.03(12)
Mes1-Mes2	rac-**1**	93.25(9)	93.23(9)	93.30(10)
	cong-*R*-**1**	95.65(8)	83.20(3)	84.18(10)
Intramolecular C-H···π (Å)				
Parameter		Sunlight	UV 365	UV 395
Distance	rac-**1**	3.2820(4)	3.2908(10)	3.2881(10)
	cong-*R*-**1**	2.9014(19)	2.9014(19)	2.9072 (3)
Intermolecular C-H···Br (Å)				
Parameter		Sunlight	UV 365	UV 395
Distance	rac-**1**	3.221(4) 3.310(5) 3.456(4)	3.2179(3) 3.3144(3) 3.4564(3)	3.2222(4) 3.3122(4) 3.4532(4)
D_{avg}	rac-**1**	3.3290	3.3296	3.3092
Distance	cong-*R*-**1**	3.2281(4) 3.5544(5)	3.2175(4) 3.5489(5)	3.2194(3) 3.5484(3)
D_{avg}	cong-*R*-**1**	3.3913	3.3832	3.3844

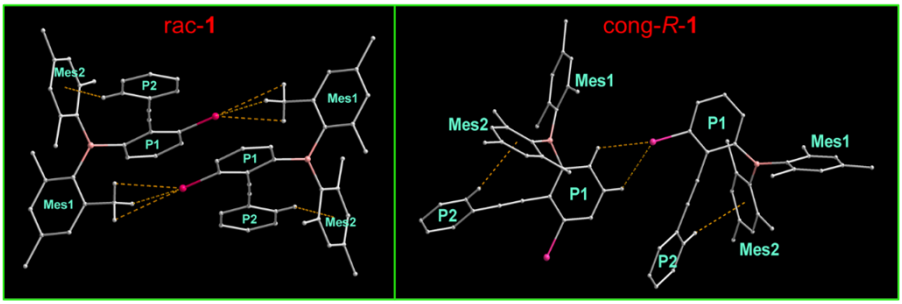

Figure S37. Simplified schematic diagram of typical dimer's bond lengths and dihedral angles in rac-**1** and cong-*R*-**1** crystals (phenyl ring: P, 2,4,6-trimethylphenyl: Mes), no intra/intermolecular interactions of H atoms in the structures were omitted for clarity.

Table. S10 Selected bond lengths (Å) and angles (deg) for rac-**1**-sunlight.

B1−C5	1.577(3)	B1−C15	1.571(3)
B1−C24	1.570(3)	Br1−C1	1.888(3)
C15−B1−C5	120.7(2)	C24−B1−C5	115.14(19)
C24−B1−C15	124.1(2)	C2−C1−Br1	118.2(2)
C6−C1−Br1	120.15(19)		

Table. S11 Selected bond lengths (Å) and angles (deg) for rac-**1**-365nmUV.

B1−C14	1.576(3)	B1−C15	1.573(3)
B1−C24	1.573(3)	Br1−C10	1.892(3)
C15−B1−C14	115.51(19)	C24−B1−C15	123.8(2)
C24−B1−C14	120.7(2)	C9−C10−Br1	120.07(18)
C11−C10−Br1	118.2(2)		

Table. S12 Selected bond lengths (Å) and angles (deg) for rac-**1**-395nmUV.

B1−C10	1.576(4)	B1−C15	1.575(4)
B1−C24	1.567(3)	Br1−C14	1.888(3)
C24−B1−C10	121.0(2)	C15−B1−C10	115.1(2)
C24−B1−C15	123.9(2)	C9−C14−Br1	120.24(19)
C13−C14−Br1	118.3(2)		

Table. S13 Selected bond lengths (Å) and angles (deg) for cong-*R*-**1**-sunlight.

B1−C14	1.583(4)	B1−C15	1.569(4)
B1−C24	1.604(4)	Br1−C10	1.906(3)
C15−B1−C5	122.52(19)	C24−B1−C5	117.76(19)
C24−B1−C15	119.64(18)	C9−C14−Br1	124.1(2)
C13−C14−Br1	117.5(2)		

Table. S14 Selected bond lengths (Å) and angles (deg) for cong-*R*-**1**-365nmUV.

B1−C10	1.572(4)	B1−C15	1.575(4)
B1−C30	1.607(4)	Br1−C14	1.899(3)
C3−B1−C15	122.8(2)	C3−B1−C24	117.8(2)
C15−B1−C24	119.3(2)	C2−C1−Br1	120.0(2)
C6−C1−Br1	117.5(2)		

Table. S15 Selected bond lengths (Å) and angles (deg) for cong-*R*-**1**-395nmUV.

B1−C5	1.570(4)	B1−C15	1.577(4)
B1−C24	1.582(4)	Br1−C1	1.901(3)
C5−B1−C15	122.6(2)	C5−B1−C24	118.0(2)
C15−B1−C24	119.4(2)	C2−C1−Br1	117.4(2)
C6−C1−Br1	119.9(2)		

Table. S16 Selected bond lengths (Å) and angles (deg) for cong-*S*-**1**-sunlight.

B1−C14	1.578(4)	B1−C15	1.583(4)
B1−C30	1.572(5)	Br1−C10	1.901(3)
C14−B1−C15	117.7(3)	C30−B1−C14	122.6(3)
C30−B1−C15	119.6(3)	C9−C10−Br1	119.8(2)
C11−C10−Br1	117.8(2)		

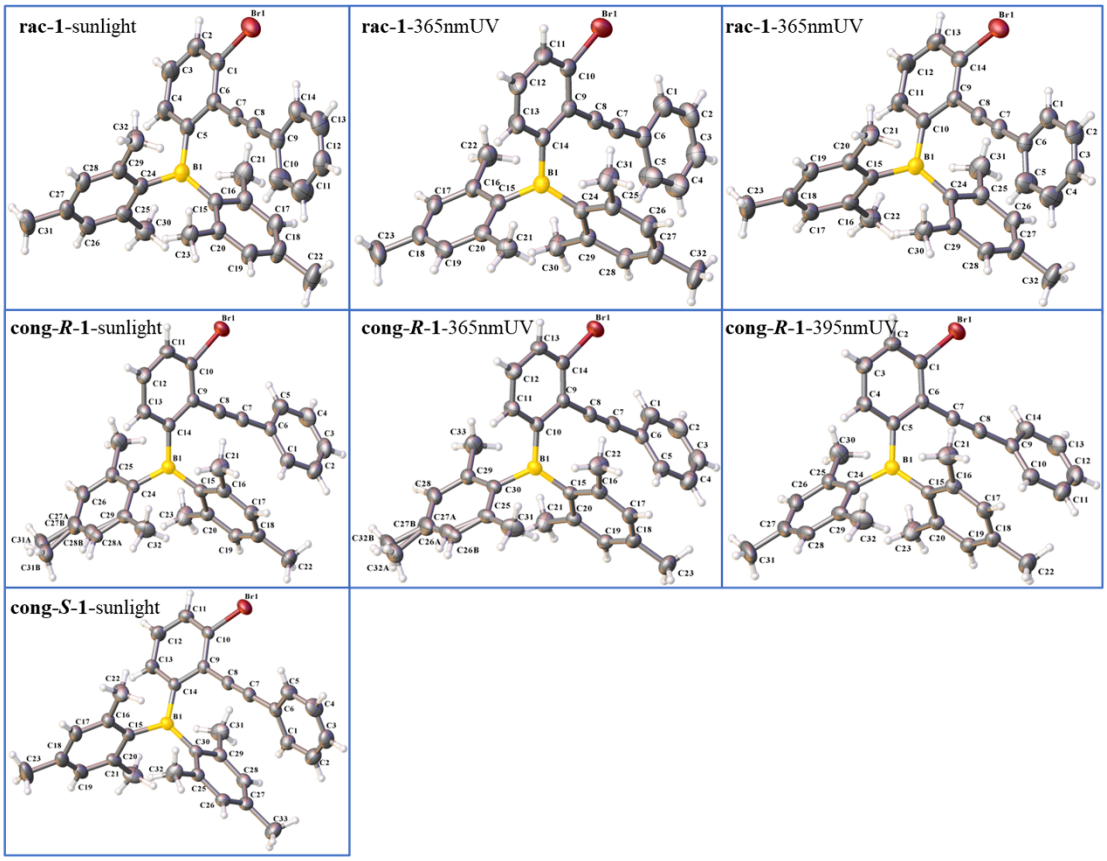

Figure S38. Thermal ellipsoid diagram of rac-**1** (sunlight, 365nmUV, 395nmUV), cong-*R*-**1** (sunlight, 365nmUV, 395nmUV) and cong-*S*-**1** (sunlight), ellipticity is 30%.

Time-dependent density functional theory (TD-DFT) calculations

When T_n contains the same transition orbital compositions as S_1 and its energy level lies with $E_{S1} \pm 0.3$ eV, the singlet-to-triplet transition from S_1 to T_n is considered to be the possible channels for the intersystem crossing. The geometries of the monomers and dimers are obtained from the crystals. The electronic state transitions and configuration coefficients were calculated using time-dependent DFT (TD-DFT) at PBE0-D3(BJ)/def2SVP level. The RI auxiliary basis set was chosen as Def2/J.[6] All the quantum chemical simulations including the energies of excited states and the spin-orbital coupling were conducted with ORCA.[7] The molecular orbitals are visually demonstrated using VMD software.[8]

TD-DFT calculations were performed on Gaussian 09 program (Revision D. 01).[9] In consideration of slight difference between three conformations under the corresponding conditions, we speculate that optimized structure could not describe experiment conclusion suitably, therefore, the SCXRD structures were used to calculated excitation energies. The excitation energies in the *n*-th singlet (S_n) and *n*-th triplet (T_n) states were obtained using the TD-PBE0/6-311G* method based on the three structures under different test conditions at room temperature (sun light; UV 365; UV 395). TD-B3LYP/6-311* method also be tried to obtain excitation energies, unfortunately, the calculated results cannot be well matched the experimental results.

rac-1 (monomer)	Transition (%)	
T_1	H → L+1 (24.2)	(n, π*)
	H → L (52.3)	(π, π*)

cong-*R*-1 (monomer)	Transition (%)	
T_1	H → L (10.7)	(n, π*)
	H-1 → L (59.9)	(π, π*)

cong-*R*-1 (dimer)	Transition (%)	
T_1	H → L+3 (27.8)	(π, π*)
	H → L+1 (40.5)	(n, π*)

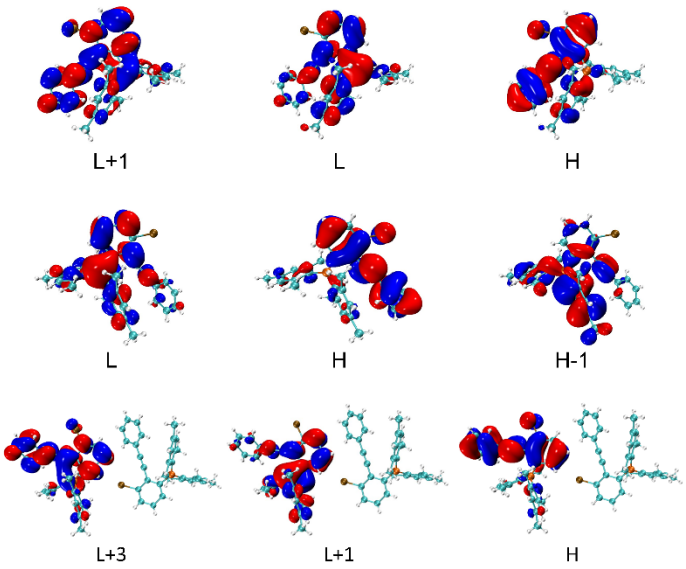

Figure S39. The corresponding frontier molecular orbitals of rac-**1** and cong-*R*-**1** based on B3LYP/6-31(d) level corresponding to its monomer and dimers.

Table S17. TD-DFT-calculated energy levels at spin-orbit coupling (SOC) results between S_1 and T_n of rac-**1** and cong-*R*-**1** (Red marks are available ISC channel).

$\langle S_1\|\hat{H}_{soc}\|T_n\rangle$/cm^{-1}	rac-1 (monomer)	rac-1 (dimer)	cong-*R*-1 (monomer)	cong-*R*-1 (dimer)
T_1-S_0	0.97	0.11	3.73	4.10
S_1-T_1	3.29	0.10	3.58	0.08
S_1-T_2	3.83	3.63	1.64	3.13
S_1-T_3	5.45	1.46	3.22	1.51
S_1-T_4	7.79	5.78	2.66	0.06
S_1-T_5	4.53	4.79	24.49	3.11
S_1-T_6	8.91	5.19	4.30	0.05
S_1-T_7	1.19	5.86	1.13	0.07
S_1-T_8	10.72	0.02	14.81	2.69
S_1-T_9		0.06		0.11
S_1-T_{10}		1.87		12.05
S_1-T_{11}		3.49		20.76
S_1-T_{12}		0.32		0.06
S_1-T_{13}		0.08		1.13
S_1-T_{14}		5.16		0.01
S_1-T_{15}		0.42		1.22
S_1-T_{16}		12.41		13.69

Table S18. The singlet and triplet excited states transition configurations of rac-**1**-sunlight monomer revealed by TD-DFT calculations. The matched excited states that contain the same orbital transition components of S_1 were highlighted in red.

	n-th	Energy (eV)	Transition configuration (%)
S_n	1	3.5480	H-1→L(24.4), H→L(71.2)
	2	3.6180	H-1→L(69.8), H→L(21.4), H-3→L(3.9), H-1→L+1(1.1)
T_n	1	2.7180	H→L(52.3), H→L+1(24.2), H-5→L+2(3.5), H-5→L(2.7), H-1→L+1(1.8), H-6→L+3(1.7), H-3→L+1(1.6), H-8→L(1.5), H-8→L+5(1.5)
	2	3.0200	H-1→L(35.5), H-3→L(18.6), H-2→L(7.1), H→L+1(6.9), H→L(3.0), H-4→L+7(2.8), H-1→L+2(2.5), H-3→L+2(2.3), H-4→L+6(2.2), H-1→L+1(2.2), H-3→L+4(2.0), H-5→L(1.4), H-3→L+1(1.0), H-4→L+8(1.0)
	3	3.2090	H-1→L(27.7), H-3→L(23.0), H-1→L+4(10.8), H-2→L(4.5), H-1→L+1(4.3), H-3→L+1(4.1), H-2→L+6(3.8), H-2→L+5(2.2), H-3→L+2(2.0), H-3→L+4(2.0), H-2→L+7(2.0), H-1→L+7(1.3), H-2→L+8(1.2)
	4	3.5350	H-5→L(24.8), H-6→L+3(12.6), H→L+1(10.3), H-5→L+2(7.9), H-8→L(7.6), H-5→L+1(6.8), H→L+5(6.5), H-7→L(2.9), H-8→L+1(2.7), H-1→L+2(1.7)
	5	3.5870	H-4→L(50.3), H→L(13.8), H→L+1(8.5), H-1→L(4.6), H-4→L+2(3.4), H-3→L(3.2), H-4→L+1(2.6), H-5→L(2.3), H-5→L+2(1.7), H-4→L+4(1.2), H-3→L+1(1.0)
	6	3.6620	H-4→L(31.8), H→L(18.9), H→L+1(13.6), H-5→L(7.0), H-5→L+2(4.2), H-3→L(3.3), H-6→L+3(2.8), H-4→L+1(2.8), H→L+2(1.5), H-3→L+1(1.5), H-1→L(1.1)
	7	3.7480	H-2→L(70.0), H-3→L(14.3), H-2→L+1(5.4), H-2→L+4(3.8), H-3→L+1(1.0)
	8	3.8070	H-5→L(19.6), H-1→L(9.6), H-6→L+3(7.3), H-5→L+1(6.8), H-1→L+1(5.5), H-2→L+5(4.4), H→L+2(4.3), H→L+1(4.1), H-8→L+1(3.6), H→L+5(3.3), H-2→L+6(2.9), H-1→L+4(2.8), H→L(2.4), H-3→L+6(1.9), H-3→L(1.7), H-2→L+7(1.5), H-3→L+8(1.2), H-3→L+4(1.2)
	9	3.8580	H-5→L(15.8), H-1→L(11.5), H-3→L(10.5), H-2→L+6(9.3), H-1→L+4(5.9), H-2→L+5(4.7), H-6→L+3(4.6), H-2→L+7(3.7), H-2→L+8(3.1), H→L+5(2.4), H→L+1(2.2), H-3→L+6(2.0), H-5→L+1(2.0), H-3→L+5(2.0), H-3→L+4(2.0), H-8→L+1(1.7), H-2→L+4(1.1), H-3→L+8(1.1), H-4→L(1.0)
	10	4.0480	H-3→L(15.6), H-4→L+7(12.4), H-4→L+6(11.6), H-1→L+1(5.2), H-4→L+8(4.5), H→L+1(4.4), H-5→L(4.2), H-2→L(4.1), H-1→L(4.0), H-3→L+1(2.6), H-1→L+2(2.1), H-3→L+2(2.1), H-7→L(1.6), H-1→L+4(1.4), H-7→L+1(1.3), H-4→L+4(1.3), H-3→L+10(1.2), H-3→L+4(1.2), H-5→L+2(1.2), H-6→L+3(1.1)

Table S19. The singlet and triplet excited states transition configurations of rac-**1**-sunlight dimer revealed by TD-DFT calculations. The matched excited states that contain the same orbital transition components of S_1 were highlighted in red.

	n-th	Energy (eV)	Transition configuration (%)
S_n	1	3.5000	H→L(60.7), H-1→L+1(32.2), H-2→L(2.6)
	2	3.5130	H→L+1(48.0), H-1→L(39.6), H-2→L+1(4.8), H-3→L(1.6)
T_n	1	2.6950	H-1→L(26.5), H→L+1(24.5), H→L+2(16.1), H-1→L+3(10.0), H-11→L+1(1.9), H-10→L+4(1.7), H-11→L+5(1.5), H-3→L+3(1.3)
	2	2.7000	H→L(26.9), H-1→L+1(24.8), H→L+3(14.5), H-1→L+2(10.7), H-11→L(2.1), H-11→L+4(1.5), H-3→L+2(1.4), H-10→L+5(1.3)
	3	3.0240	H-2→L+1(20.4), H-3→L(11.2), H-2→L(6.1), H-4→L+1(5.7), H-7→L(5.6), H-5→L(5.2), H-6→L+1(4.4), H-1→L+3(3.3), H-1→L(3.0), H→L+2(2.8), H-9→L+15(1.9), H-2→L+5(1.5), H-8→L+14(1.5), H-2→L+2(1.4), H-8→L+13(1.2), H-10→L(1.1)
	4	3.0240	H-3→L+1(16.9), H-2→L(14.6), H-3→L(6.5), H-7→L+1(5.7), H-4→L(5.6), H-5→L+1(5.2), H-6→L (4.3), H-1→L+2(3.3), H-1→L+1(3.1), H→L+3(2.7), H-8→L+15(1.8), H-9→L+14(1.6), H-2→L+3(1.3), H-3→L+5(1.1), H-8→L+12(1.1), H-9→L+13(1.1), H-2→L+4(1.0), H-10→L+1(1.0)
	5	3.2220	H-2→L+1(9.8), H-2→L(9.3), H-2→L+8(6.3), H-7→L(4.9), H-6→L+1(4.5), H-7→L+1(4.1), H-4→L+1(4.0), H-6→L(3.8), H-4→L(3.4), H-2→L+9(2.9), H-3→L(2.9), H-5→L(2.5), H-5→L+1(2.1), H-3→L+1(1.9), H-2→L+2(1.5), H-2→L+3(1.5), H-3→L+8(1.4), H-7→L+3(1.0)
	6	3.2220	H-3→L+1(10.7), H-3→L(10.2), H-3→L+9(6.6), H-7→L+1(5.2), H-7→L(4.4), H-6→L(4.2), H-4→L(3.9), H-6→L+1(3.5), H-4→L+1(3.2), H-5→L+1(2.7), H-3→L+8(2.6), H-5→L(2.3), H-2→L(1.8), H-3→L+2(1.7), H-3→L+3(1.6), H-2→L+1(1.1), H-2→L+9(1.0)
	7	3.4970	H-10→L+1(15.6), H-11→L(15.1), H→L(8.1), H-10→L+5(5.1), H-11→L+4(4.1), H-12→L+7(3.2), H-16→L+1(3.1), H-10→L+2(2.8), H-13→L+6(2.8), H-17→L(2.6), H-1→L+2(2.6), H-14→L(2.2), H-11→L+3(2.0), H-1→L+11(1.7), H→L+10(1.5), H→L+3(1.2), H-6→L(1.1), H-16→L+2(1.1), H-1→L+1(1.1)
	8	3.5100	H-10→L(17.7), H-11→L+1(13.7), H→L+1(5.4), H-10→L+4(4.5), H-16→L(3.8), H-11→L+5(3.8), H-12→L+6(3.6), H-11→L+2(3.4), H-13→L+7(3.2), H→L+2(2.9), H-17→L+1(2.6), H-1→L+3(2.3), H-14→L+1(2.2), H-1→L+10(2.0), H→L+11(1.9), H-10→L+3(1.8), H-1→L(1.1), H-16→L+3(1.1)
	9	3.5610	H→L+1(24.7), H→L+2(16.7), H-1→L+3(8.3), H-8→L+1(6.8), H-9→L(6.3), H-1→L(6.2), H-3→L(2.4), H-12→L+6(2.2), H-13→L+7(2.1), H-7→L(2.1), H-10→L+4(1.2), H-2→L+1(1.1), H-10→L(1.0)
	10	3.5630	H→L(24.5), H→L+3(13.0), H-1→L+2(12.5), H-8→L(7.0), H-9→L+1(6.2), H-1→L+1(5.2), H-12→L+7(2.4), H-13→L+6(2.2), H-3→L+1(2.0), H-7→L+1(1.7), H-2→L(1.0), H-3→L+2(1.0)
	11	3.6380	H-8→L(33.8), H-9→L+1(32.7), H→L(6.0), H-8→L+3(2.3), H-9→L+2(2.2),

			H-4→L(1.9), H-1→L+2(1.9), H→L+3(1.7), H-9→L+5(1.3), H-8→L+4(1.3)
	12	3.6380	H-9→L(33.9), H-8→L+1(32.8), H→L+1(5.8), H→L+2(2.6), H-9→L+3(2.5), H-8→L+2(1.9), H-4→L+1(1.9), H-8→L+5(1.3), H-9→L+4(1.3), H-10→L(1.1), H-9→L+8(1.1), H-1→L+3(1.0)
	13	3.7680	H-1→L(14.7), H→L+2(7.4), H-10→L(7.4), H-11→L+1(7.1), H-10→L+3(4.9), H-11→L+2(4.9), H-12→L+6(4.6), H-13→L+7(4.4), H→L+11(3.3), H-1→L+4(2.5), H-16→L+3(2.4), H-17→L+2(2.2), H→L+5(2.0), H-3→L+3(1.8), H-10→L+4(1.7), H-5→L(1.7), H→L+1(1.6), H-2→L+2(1.4), H-1→L+10(1.4), H→L+13(1.3)
	14	3.7790	H-5→L+1(19.8), H-4→L(15.7), H-6→L(13.2), H-7→L+1(8.6), H-1→L+1(2.7), H→L+3(2.5), H-11→L(2.3), H-10→L+2(2.2), H-10→L+1(2.1), H-5→L+2(2.0), H-4→L+3(1.9), H→L+4(1.7), H-12→L+7(1.4), H-13→L+6(1.3), H-11→L+3(1.3), H-6→L+8(1.1)
	15	3.7800	H-5→L(26.1), H-4→L+1(20.7), H-6→L+1(19.5), H-7→L(15.3), H-5→L+3(1.8), H-5→L+8(1.8), H-6→L+2(1.7), H-4→L+9(1.5), H-7→L+3(1.4), H-4→L+2(1.3), H-9→L(1.0)
	16	3.7830	H-6→L(7.8), H-1→L+1(7.7), H-10→L+1(7.6), H-11→L(6.8), H-4→L(6.7), H-5→L+1(6.2), H-7→L+1(6.0), H→L+3(4.4), H-10→L+2(3.3), H-12→L+7(3.0), H→L+4(2.9), H-13→L+6(2.8), H-11→L+3(2.1), H-16→L+2(1.8), H-3→L+2(1.6), H→L+10(1.5), H-4→L+8(1.4), H-7→L+2(1.3), H-17→L+3(1.2), H-5→L+9(1.2), H-6→L+3(1.2), H-1→L+11(1.2)
	17	3.8610	H-3→L(11.6), H-2→L+1(7.1), H-7→L(4.2), H-6→L+1(4.1), H-5→L+10(4.0), H-4→L+11(3.9), H-5→L+12(3.5), H-6→L+11(3.4), H-6→L+13(3.1), H→L+1(3.1), H-7→L+10(2.9), H-3→L+8(2.5), H-5→L+15(2.5), H-4→L+14(2.5), H-7→L+12(2.4), H-4→L+9(2.4), H-2→L+9(2.3), H-1→L(2.1), H-2→L(2.1), H-4→L+1(2.0), H-4→L+13(1.9), H-5→L+8(1.9), H-6→L+14(1.4), H-2→L+8(1.2), H-8→L+1(1.0), H-9→L(1.0)
	18	3.8630	H-3→L+1(9.5), H-2→L(8.1), H-5→L+11(4.4), H-6→L(4.4), H-7→L+1(3.9), H-6→L+10(3.8), H-3→L+9(3.5), H-2→L+8(3.1), H-4→L+10(3.0), H-5→L+14(3.0), H-6→L+12(3.0), H-4→L+12(2.9), H-7→L+11(2.6), H-1→L+1(2.6), H-5→L+13(2.5), H-7→L+13(2.4), H-4→L+8(2.3), H-4→L+15(2.2), H-4→L(2.2), H→L(2.2), H-5→L+9(1.8), H-3→L(1.5), H-2→L+1(1.3), H-8→L(1.2), H-9→L+1(1.0)

Table S20. The singlet and triplet excited states transition configurations of cong-*R*-**1**-sunlight monomer revealed by TD-DFT calculations. The matched excited states that contain the same orbital transition components of S_1 were highlighted in red.

	n-th	Energy (eV)	Transition configuration (%)
S_n	1	3.5060	H-1→L(87.9), H→L(8.3), H-3→L(1.1)
	2	3.5950	H→L(82.5), H-1→L(9.2), H-3→L(4.8)
T_n	1	2.7230	H→L(37.4), H→L+1(26.4), H-1→L(10.9), H-7→L(5.7), H-5→L+2(3.5), H-7→L+4(1.8), H-1→L+1(1.7), H-6→L+3(1.3), H-5→L(1.0)
	2	3.0260	H-1→L(59.9), H→L(10.7), H-1→L+1(4.1), H-1→L+2(3.7), H-2→L+6(3.2), H-1→L+5(3.1), H-3→L+5(2.0), H-2→L+7(1.6), H-4→L+7(1.4)
	3	3.1620	H-3→L(57.9), H-3→L+4(6.6), H-3→L+1(5.5), H-3→L+5(4.3), H-4→L+6(3.8), H-1→L+5(2.8), H-4→L+7(2.3), H-2→L+7(2.3), H→L+1(1.8), H→L(1.1)
	4	3.3650	H→L+1(16.3), H-7→L(14.9), H-6→L+3(11.4), H-5→L+1(10.9), H→L+2(9.1), H→L+4(8.2), H-5→L+4(2.0), H-7→L+1(1.8), H-3→L+1(1.6), H-8→L(1.5), H-7→L+2(1.2), H-8→L+1(1.1), H-3→L+2(1.1), H-1→L+5(1.0)
	5	3.5190	H-5→L(33.9), H→L(26.9), H→L+1(7.6), H-5→L+2(6.3), H-2→L(4.0), H-7→L(3.5), H-1→L(2.2), H-5→L+1(1.8), H-3→L(1.8), H-5→L+4(1.3), H-12→L(1.3), H→L+4(1.2)
	6	3.5720	H-2→L(81.7), H-2→L+1(2.8), H-2→L+2(2.3), H-4→L(2.0), H-2→L+5(1.6), H→L(1.3), H-5→L(1.3), H-4→L+5(1.2)
	7	3.6770	H-4→L(82.2), H-4→L+1(4.7), H-4→L+4(3.3), H-2→L(1.9), H-2→L+5(1.3), H-3→L(1.1), H-4→L+5(1.1)
	8	3.7370	H-5→L(35.3), H→L+1(16.8), H→L(11.1), H-5→L+1(9.5), H-1→L+1(6.8), H→L+2(6.4), H-7→L+1(2.1), H-5→L+2(1.1)
	9	3.8390	H-1→L(20.0), H-2→L+6(16.7), H-4→L+7(8.4), H-2→L+7(7.0), H-1→L+2(5.8), H-3→L+5(3.8), H-1→L+5(3.5), H-1→L+1(2.6), H-2→L+5(2.5), H-5→L+1(2.4), H-1→L+10(1.9), H→L(1.9), H-6→L+3(1.5), H→L+1(1.3), H-1→L+6(1.3), H-1→L+4(1.2), H-10→L(1.2), H→L+4(1.1), H-2→L+2(1.1), H-2→L+3(1.0)
	10	3.9250	H-3→L(30.6), H-4→L+6(14.9), H-2→L+7(9.5), H-4→L+7(9.3), H-3→L+5(5.3), H-4→L+5(5.1), H-3→L+4(4.0), H-1→L+5(2.6), H-3→L+10(2.5), H-4→L+4(1.8), H-4→L(1.2), H→L+5(1.0)

Table S21. The singlet and triplet excited states transition configurations of cong-*R*-**1**-sunlight dimer revealed by TD-DFT calculations. The matched excited states that contain the same orbital transition components of S_1 were highlighted in red.

	n-th	Energy (eV)	Transition configuration (%)
S_n	1	3.4980	H-5→L(72.5), H-2→L(17.1), H-4→L(6.5), H-8→L(1.0)
	2	3.5330	H-1→L+1(92.5), H→L+1(3.7)
T_n	1	2.7360	H→L+1(40.5), H→L+3(27.8), H-1→L+1(7.5), H-13→L+1(4.5), H-10→L+5(2.7), H-10→L+1(1.4)
	2	2.7420	H-2→L(31.0), H-2→L+2(23.4), H-5→L(16.4), H-15→L(6.1), H-5→L+2(3.7), H-11→L+4(3.5), H-15→L+7(1.8), H-11→L+2(1.0)
	3	3.0250	H-5→L(48.2), H-2→L(19.0), H-4→L(4.4), H-5→L+2(4.0), H-7→L+12(2.6), H-5→L+4(2.6), H-5→L+10(1.7), H-9→L+14(1.6), H-8→L+10(1.5), H-7→L+14(1.2)
	4	3.0440	H-1→L+1(64.3), H→L+1(6.6), H-1→L+11(3.7), H-1→L+3(3.5), H-1→L+5(2.7), H-3→L+15(2.2), H-6→L+17(1.7), H-4→L+11(1.5), H-3→L+17(1.2)
	5	3.1540	H-8→L(59.3), H-8→L+7(6.5), H-8→L+2(5.0), H-9→L+12(3.1), H-8→L+10(2.6), H-7→L+14(2.5), H-9→L+14(2.2), H-2→L+2(1.9), H-2→L(1.7), H-5→L+10(1.5)
	6	3.1700	H-4→L+1(54.6), H-4→L+3(4.4), H-5→L+1(4.3), H-6→L+15(4.1), H-4→L+8(3.7), H-3→L+17(2.6), H-1→L+11(2.2), H-6→L+17(1.8), H-4→L+13(1.7), H→L+3(1.7), H-4→L+10(1.6), H-1→L+8(1.1), H-4→L+16(1.0)
	7	3.3810	H→L+3(17.0), H-13→L+1(12.1), H-10→L+3(9.8), H-12→L+9(9.7), H→L+8(6.6), H→L+5(5.6), H-13→L+3(2.2), H-12→L+1(1.9), H→L+10(1.7), H-13→L+9(1.7), H-10→L+1(1.5), H→L+1(1.5), H-16→L+1(1.4), H-4→L+3(1.3), H→L+11(1.3), H-12→L+8(1.3), H-16→L+3(1.2), H-14→L+1(1.0)
	8	3.3890	H-2→L+2(16.2), H-15→L(15.2), H-11→L+2(10.2), H-14→L+6(10.0), H-2→L+4(9.4), H-2→L+7(6.5), H-15→L+2(2.1), H-11→L+7(2.0), H-8→L+2(1.8), H-5→L+7(1.4), H-15→L+4(1.4), H-17→L(1.4), H-8→L+4(1.2), H-13→L+6(1.1), H-17→L+2(1.0)
	9	3.5270	H-10→L+1(35.2), H→L+1(28.7), H→L+3(7.2), H-10→L+5(5.2), H-3→L+1(3.2), H-13→L+1(2.5), H-4→L+1(2.0), H-10→L+3(1.4)
	10	3.5360	H-7→L(67.4), H-11→L(8.2), H-2→L(5.9), H-7→L+2(2.1), H-15→L(1.8), H-9→L(1.6), H-11→L+4(1.5), H-2→L+2(1.0), H-7→L+4(1.0)
	11	3.5610	H-11→L(27.6), H-2→L(19.0), H-7→L(18.0), H-2→L+2(6.0), H-11→L+4(4.3), H-5→L(3.9), H-8→L(2.5), H-15→L(1.7), H-2→L+7(1.4), H-9→L(1.3), H-11→L+2(1.0)
	12	3.5850	H-3→L+1(81.7), H-6→L+1(3.4), H-3→L+3(2.6), H-3→L+11(1.7), H-3→L+5(1.6), H-6→L+11(1.2), H→L+1(1.2), H-10→L+1(1.1)
	13	3.6400	H-9→L(82.2), H-9→L+2(4.3), H-9→L+7(3.0), H-7→L(2.5), H-8→L(2.0)
	14	3.6750	H-6→L+1(82.0), H-6→L+3(3.9), H-3→L+1(3.2), H-6→L+8(1.6), H-4→L+1(1.2)

	15	3.7550	H-10→L+1(33.5), H→L+3(17.9), H→L+1(10.9), H-10→L+3(9.8), H→L+5(5.8), H-1→L+3(4.4), H-13→L+3(2.2), H→L+8(1.4), H-12→L+9(1.2)
	16	3.7660	H-11→L(32.3), H-2→L+2(13.5), H-2→L(11.1), H-11→L+2(9.5), H-5→L+2(8.9), H-2→L+4(5.6), H-15→L+2(2.3), H→L(1.9), H-11→L+4(1.2)
	17	3.8600	H-5→L(16.1), H-7→L+12(14.9), H-9→L+14(9.8), H-5→L+4(5.3), H-7→L+14(5.1), H-7→L+13(3.8), H-8→L+10(3.2), H-2→L(3.1), H-11→L+2(2.4), H-2→L+2(2.2), H-5→L+2(2.0), H-5→L+10(2.0), H-7→L+10(1.9), H-5→L+19(1.6), H-4→L(1.4), H-2→L+7(1.4), H-14→L+6(1.2), H-21→L(1.1), H-7→L+6(1.1)
	18	3.8770	H-1→L+1(20.9), H-3→L+15(12.0), H-6→L+17(9.9), H-3→L+17(4.9), H-1→L+11(4.6), H-3→L+13(4.6), H-1→L+5(4.0), H-1→L+3(3.0), H-4→L+11(2.7), H-3→L+16(2.1), H-1→L+22(1.9), H-10→L+3(1.8), H-3→L+9(1.6), H-3→L+12(1.2), H→L+1(1.1), H-19→L+1(1.0), H-1→L+10(1.0)

Table S22. The singlet and triplet excited states transition configurations of rac-**1**-sunlight dimer revealed by TD-DFT calculations. The matched excited states that contain the same orbital transition components of S_1 were highlighted in red.

	n-th	Energy (eV)	Transition configuration (%)
S_n	1	3.5008	H-2→L(2.66), H-1→L+1(32.23), H→L(60.65)
	2	3.5138	H-2→L+1(4.82), H-1→L(39.63), H→L+1(47.94)
T_n	1	2.6968	H-1→L(26.88), H-1→L+3(10.34), H→L+1(24.82), H→L+2(16.55)
	2	2.7021	H-11→L(2.13), H-1→L+1(25.15), H-1→L+2(11.02), H→L(27.17), H→L+3(14.86)
	3	3.0241	H-9→L+15(2.13), H-7→L(5.56), H-6→L+1(4.33), H-5→L(5.22), H-4→L+1(5.69), H-3→L(11.31), H-2→L(6.22), H-2→L+1(20.54), H-1→L(3.03), H-1→L+3(3.39), H→L+2(2.83)
	4	3.0245	H-8→L+15(2.05), H-7→L+1(5.65), H-6→L(4.24), H-5→L+1(5.28), H-4→L(5.62), H-3→L(6.62), H-3→L+1(17.12), H-2→L(14.71), H-1→L+1(3.09), H-1→L+2(3.38), H→L+3(2.71)
	5	3.222	H-7→L(5.15), H-7→L+1(3.97), H-6→L(3.64), H-6→L+1(4.69), H-5→L(2.67), H-5→L+1(2.05), H-4→L(3.28), H-4→L+1(4.22), H-3→L(3.03), H-2→L(9.09), H-2→L+1(9.79), H-2→L+8(5.87), H-2→L+9(3.71)
	6	3.2222	H-7→L(4.25), H-7→L+1(5.45), H-6→L(4.42), H-6→L+1(3.36), H-5→L(2.22), H-5→L+1(2.83), H-4→L(4.06), H-4→L+1(3.08), H-3→L(9.92), H-3→L+1(10.79), H-3→L+8(3.22), H-3→L+9(6.45)
	7	3.4982	H-17→L(2.66), H-16→L+1(3.15), H-14→L(2.23), H-13→L+6(2.95), H-12→L+7(3.28), H-11→L(15.33), H-11→L+4(4.27), H-10→L+1(15.84), H-10→L+2(2.89), H-10→L+5(5.31), H-1→L+2(2.5), H→L(8.33)
	8	3.5121	H-17→L+1(2.6), H-16→L(3.77), H-14→L+1(2.23), H-13→L+7(3.23), H-12→L+6(3.7), H-11→L+1(14.03), H-11→L+2(3.4), H-11→L+5(3.93), H-10→L(18.03), H-10→L+4(4.71), H-1→L+3(2.15), H-1→L+10(2.01), H→L+1(5.86), H→L+2(2.75)
	9	3.5619	H-13→L+7(2.27), H-12→L+6(2.4), H-9→L(6.42), H-8→L+1(6.87), H-7→L(2.03), H-3→L(2.44), H-1→L(6.26), H-1→L+3(8.51), H→L+1(24.21), H→L+2(16.96)
	10	3.5636	H-13→L+6(2.36), H-12→L+7(2.59), H-9→L+1(6.34), H-8→L(7.1), H-3→L+1(2.03), H-1→L+1(5.18), H-1→L+2(12.7), H→L(24.1), H→L+3(13.12)
	11	3.6382	H-9→L+1(32.61), H-9→L+2(2.2), H-8→L(33.63), H-8→L+3(2.28), H→L(6.05)
	12	3.6388	H-9→L(33.84), H-9→L+3(2.51), H-8→L+1(32.69), H→L+1(5.85),H→L+2(2.67)
	13	3.7689	H-17→L+2(2.24), H-16→L+3(2.48), H-13→L+7(4.63), H-12→L+6(4.83), H-11→L+1(7.01), H-11→L+2(4.92), H-10→L(7.25), H-10→L+3(5.02), H-1→L(14.68), H-1→L+4(2.47), H→L+2(7.34), H→L+11(3.35)
	14	3.7792	H-7→L+1(10.22), H-6→L(15.41), H-5→L+1(22.06), H-5→L+2(2.14), H-4→L(17.84)
	15	3.7805	H-7→L(15.35), H-6→L+1(19.57), H-5→L(25.86), H-4→L+1(20.46)
	16	3.7837	H-16→L+2(2.08), H-13→L+6(3.33), H-12→L+7(3.61), H-11→L(7.61),

			H-11→L+3(2.46), H-10→L+1(8.43), H-10→L+2(3.93), H-7→L+1(4.5), H-6→L(5.64), H-5→L+1(3.83), H-4→L(4.45), H-1→L+1(8.71), H→L+3(5.14), H→L+4(3.38)
	17	3.8608	H-7→L(4.24), H-7→L+10(3.01), H-7→L+12(2.45), H-6→L+1(4.09), H-6→L+11(3.51), H-6→L+13(3.23), H-5→L+10(4.06), H-5→L+12(3.6), H-5→L+15(2.6), H-4→L+1(2.03), H-4→L+9(2.5), H-4→L+11(3.94), H-4→L+14(2.59), H-3→L(11.6), H-3→L+8(2.82), H-2→L(2.06), H-2→L+1(7.09), H-2→L+9(2.52), H-1→L(2.12), H→L+1(3.06)

Table S23. The singlet and triplet excited states transition configurations of rac-**1**-365nmUV dimer revealed by TD-DFT calculations. The matched excited states that contain the same orbital transition components of S_1 were highlighted in red.

	n-th	Energy (eV)	Transition configuration (%)
S_n	1	3.5181	H-3→L(2.46), H-1→L+1(31.63), H→L(61.76)
	2	3.5323	H-3→L+1(4.6), H-1→L(38.92), H→L+1(49.49)
T_n	1	2.7101	H-1→L(26.47), H-1→L+3(10.94), H→L+1(24.36), H→L+2(16.96)
	2	2.7154	H-11→L(2.11), H-1→L+1(24.8), H-1→L+2(11.66), H→L(26.62), H→L+3(15.26)
	3	3.0638	H-9→L(7.36), H-8→L+1(5.89), H-5→L(2.48), H-4→L+1(2.5), H-3→L+1(20.03), H-2→L(17.29), H-1→L(2.6), H-1→L+3(3.08), H→L+2(2.64)
	4	3.0641	H-9→L+1(7.57), H-8→L(5.66), H-5→L+1(2.45), H-4→L(2.54), H-3→L(20.59), H-2→L+1(16.8), H-1→L+1(2.65), H-1→L+2(3.1), H→L+3(2.49)
	5	3.2479	H-9→L(10.11), H-9→L+1(2.45), H-8→L(3.05), H-8→L+1(10.41), H-5→L+11(2.51), H-4→L+10(2.02), H-3→L+1(7.64), H-3→L+8(4.04), H-2→L(10.01), H-2→L+1(2.72), H-2→L+9(4.53)
	6	3.248	H-9→L(3.17), H-9→L+1(10.84), H-8→L(9.72), H-8→L+1(2.33), H-5→L+10(2.42), H-4→L+11(2.06), H-3→L(8.24), H-3→L+1(2.27), H-3→L+9(4.2), H-2→L(2.44), H-2→L+1(9.28), H-2→L+8(4.35)
	7	3.5062	H-17→L(2.46), H-16→L+1(2.86), H-14→L(2.04), H-13→L+6(2.77), H-12→L+7(3.24), H-11→L(14.99), H-11→L+4(4.17), H-10→L+1(16.0), H-10→L+2(2.84), H-10→L+5(5.34), H→L(9.61)
	8	3.5194	H-17→L+1(2.39), H-16→L(3.38), H-14→L+1(2.02), H-13→L+7(2.99), H-12→L+6(3.62), H-11→L+1(13.7), H-11→L+2(3.39), H-11→L+5(3.85), H-10→L(18.32), H-10→L+4(4.86), H→L+1(7.29)
	9	3.557	H-9→L(2.91), H-8→L+1(6.33), H-7→L(14.45), H-6→L+1(10.25), H-2→L(3.08), H-1→L(6.25), H-1→L+3(6.64), H→L+1(15.23), H→L+2(12.44)
	10	3.5585	H-9→L+1(2.56), H-8→L(6.21), H-7→L+1(14.66), H-6→L(11.01), H-2→L+1(2.68), H-1→L+1(5.2), H-1→L+2(9.42), H→L(14.98), H→L+3(9.42)
	11	3.6205	H-12→L+7(2.09), H-7→L+1(22.39), H-6→L(20.71), H-4→L(3.12), H-1→L+2(5.75), H→L(13.8), H→L+3(5.5)
	12	3.6209	H-7→L(23.76), H-7→L+3(2.08), H-6→L+1(20.72), H-4→L+1(3.12), H-1→L+3(3.38), H→L+1(13.02), H→L+2(7.8)
	13	3.7718	H-9→L(2.79), H-7→L(2.03), H-6→L+1(6.26), H-5→L(33.6), H-5→L+3(2.74), H-4→L+1(27.99), H-4→L+2(2.62)
	14	3.7722	H-9→L+1(3.31), H-8→L(2.05), H-7→L+1(2.57), H-6→L(7.43), H-5→L+1(34.52), H-5→L+2(2.68), H-4→L(33.24), H-4→L+3(2.58)
	15	3.7776	H-16→L+3(2.06), H-13→L+7(4.56), H-12→L+6(4.96), H-11→L+1(7.36), H-11→L+2(4.22), H-10→L(7.9), H-10→L+3(3.82), H-5→L(3.16), H-4→L+1(4.15), H-1→L(12.44), H-1→L+4(2.23), H→L+2(6.15), H→L+10(2.26)
	16	3.7892	H-16→L+2(2.51), H-13→L+6(4.68), H-12→L+7(5.14), H-11→L(9.19), H-11→L+3(3.25), H-10→L+1(9.64), H-10→L+2(4.86), H-2→L+2(2.38), H-1→L+1(9.61), H→L+3(6.83), H→L+4(4.37)

	17	3.8649	H-9→L(5.51), H-8→L+1(6.81), H-5→L+11(8.95), H-5→L+15(4.07), H-4→L+10(8.1), H-4→L+14(4.72), H-3→L+1(8.42), H-3→L+8(2.87), H-2→L(12.67), H-2→L+9(3.16), H→L+1(2.44)

Table S24. The singlet and triplet excited states transition configurations of rac-**1**-395nmUV dimer revealed by TD-DFT calculations. The matched excited states that contain the same orbital transition components of S_1 were highlighted in red.

	n-th	Energy (eV)	Transition configuration (%)
S_n	1	3.5302	H-3→L(2.83), H-1→L+1(32.26), H→L(60.73)
	2	3.5424	H-3→L+1(5.24), H-1→L(39.59), H→L+1(48.24)
T_n	1	2.7313	H-11→L+1(2.32), H-10→L+4(2.11), H-1→L(26.5), H-1→L+3(10.25), H→L+1(23.37), H→L+2(16.63)
	2	2.7366	H-11→L(2.49), H-1→L+1(24.62), H-1→L+2(10.97), H→L(25.86), H→L+3(14.86)
	3	3.0662	H-8→L+13(2.01), H-7→L(8.33), H-6→L+1(8.64), H-3→L+1(20.12), H-2→L(17.55), H-1→L(2.81), H-1→L+3(3.28), H→L+2(2.75)
	4	3.0664	H-7→L+1(8.42), H-6→L(8.55), H-3→L(21.04), H-2→L+1(16.65), H-1→L+1(2.91), H-1→L+2(3.24), H→L+3(2.62)
	5	3.2384	H-7→L(8.72), H-7→L+1(4.78), H-6→L(5.1), H-6→L+1(8.92), H-5→L+10(2.25), H-4→L+11(2.08), H-3→L(3.07), H-3→L+1(5.69), H-3→L+9(3.13), H-2→L(8.46), H-2→L+1(4.77), H-2→L+8(4.06), H-2→L+9(2.06)
	6	3.2386	H-7→L(5.03), H-7→L+1(9.04), H-6→L(8.6), H-6→L+1(4.81), H-5→L+11(2.13), H-4→L+10(2.19), H-3→L(6.86), H-3→L+1(4.04), H-3→L+8(3.63), H-3→L+9(2.49), H-2→L(3.86), H-2→L+1(7.17), H-2→L+9(3.49)
	7	3.4816	H-17→L(2.18), H-16→L+1(2.71), H-14→L(2.02), H-13→L+6(2.92), H-12→L+7(3.26), H-11→L(15.71), H-11→L+4(4.27), H-10→L+1(16.89), H-10→L+2(2.55), H-10→L+5(5.2), H-6→L(2.39), H-1→L+2(2.26)
	8	3.4954	H-17→L+1(2.05), H-16→L(3.14), H-13→L+7(2.93), H-12→L+6(3.42), H-11→L+1(14.59), H-11→L+2(3.01), H-11→L+5(3.92), H-10→L(19.09), H-10→L+4(4.74), H-6→L+1(2.01), H→L+1(7.95)
	9	3.5686	H-13→L+7(2.58), H-12→L+6(2.75), H-9→L(7.48), H-8→L+1(10.58), H-7→L(4.07), H-2→L(3.1), H-1→L(6.63), H-1→L+3(7.53), H→L+1(20.1), H→L+2(14.42)
	10	3.5706	H-13→L+6(2.46), H-12→L+7(2.71), H-9→L+1(7.88), H-8→L(11.17), H-7→L+1(3.75), H-2→L+1(2.7), H-1→L+1(5.69), H-1→L+2(10.53), H→L(19.93), H→L+3(10.94)
	11	3.6385	H-9→L(8.38), H-9→L+1(19.77), H-8→L(19.77), H-8→L+1(8.21), H-1→L+2(2.26), H→L(5.97), H→L+1(2.29), H→L+3(2.04)
	12	3.6387	H-9→L(21.43), H-9→L+1(8.76), H-8→L(7.47), H-8→L+1(18.86), H→L(2.44), H→L+1(5.69), H→L+2(2.99)
	13	3.7702	H-9→L+1(2.13), H-6→L(3.31), H-5→L+1(37.05), H-5→L+2(2.48), H-5→L+9(2.43), H-4→L(38.05), H-4→L+3(2.6), H-4→L+8(2.36)
	14	3.7703	H-9→L(2.11), H-6→L+1(3.16), H-5→L(39.8), H-5→L+3(2.71), H-5→L+8(2.44), H-4→L+1(35.48), H-4→L+2(2.41), H-4→L+9(2.34)
	15	3.7837	H-17→L+2(2.17), H-16→L+3(2.46), H-13→L+7(5.45), H-12→L+6(5.75), H-11→L+1(7.22), H-11→L+2(4.53), H-10→L(7.81), H-10→L+3(4.68),

			H-2→L+3(2.07), H-1→L(12.91), H-1→L+4(2.38), H→L+2(8.32), H→L+11(2.29)
	16	3.7956	H-16→L+2(2.66), H-13→L+6(4.98), H-12→L+7(5.4), H-11→L(8.35), H-11→L+3(2.95), H-10→L+1(8.85), H-10→L+2(5.09), H-2→L+2(2.57), H-1→L+1(8.72), H→L+3(7.54), H→L+4(4.34)
	17	3.8569	H-7→L(6.31), H-6→L+1(5.53), H-5→L+10(9.77), H-5→L+12(2.88), H-5→L+15(4.07), H-4→L+11(9.43), H-4→L+14(4.87), H-3→L+1(8.32), H-3→L+9(2.85), H-2→L(12.5), H-2→L+8(3.19)

Table S25. The singlet and triplet excited states transition configurations of cong-*R*-**1**-sunlight dimer revealed by TD-DFT calculations. The matched excited states that contain the same orbital transition components of S_1 were highlighted in red.

	n-th	Energy (eV)	Transition configuration (%)
S_n	1	3.4979	H-5→L(72.92), H-4→L(6.21), H-2→L(17.09)
	2	3.5332	H-1→L+1(92.57), H→L+1(3.73)
T_n	1	2.74	H-13→L+1(4.62), H-10→L+5(3.03), H-1→L+1(7.54), H→L+1(41.08), H→L+3(28.7)
	2	2.7455	H-15→L(6.32), H-15→L+7(2.07), H-11→L+4(3.88), H-5→L(16.67), H-5→L+2(3.84), H-2→L(31.51), H-2→L+2(24.22)
	3	3.0259	H-7→L+12(2.8), H-5→L(48.66), H-5→L+2(4.05), H-5→L+4(2.67), H-4→L(4.21), H-2→L(18.94)
	4	3.0447	H-3→L+15(2.36), H-1→L+1(64.52), H-1→L+3(3.56), H-1→L+5(2.8), H-1→L+11(3.95), H→L+1(6.59)
	5	3.1579	H-9→L+12(3.29), H-9→L+14(2.4), H-8→L(59.82), H-8→L+2(5.07), H-8→L+7(6.75), H-8→L+10(2.75), H-7→L+14(2.71)
	6	3.1745	H-6→L+15(4.33), H-5→L+1(4.13), H-4→L+1(55.26), H-4→L+3(4.51), H-4→L+8(3.87), H-3→L+17(2.82), H-1→L+11(2.2)
	7	3.3844	H-13→L+1(12.28), H-13→L+3(2.3), H-12→L+9(10.53), H-10→L+3(9.96), H→L+3(17.16) H→L+5(5.74), H→L+8(6.81)
	8	3.3922	H-15→L(15.46), H-15→L+2(2.19), H-14→L+6(10.79), H-11→L+2(10.45), H-11→L+7(2.13), H-2→L+2(16.41), H-2→L+4(9.65), H-2→L+7(6.74)
	9	3.5277	H-13→L+1(2.62), H-10→L+1(35.55), H-10→L+5(5.31), H-3→L+1(3.28), H→L+1(28.42), H→L+3(7.18)
	10	3.5368	H-11→L(8.1), H-7→L(67.88), H-7→L+2(2.08), H-2→L(5.69)
	11	3.5618	H-11→L(28.08), H-11→L+4(4.48), H-8→L(2.52), H-7→L(17.48), H-5→L(3.94), H-2→L(19.04), H-2→L+2(6.14)
	12	3.5851	H-6→L+1(3.42), H-3→L+1(81.6), H-3→L+3(2.57)
	13	3.6402	H-9→L(82.25), H-9→L+2(4.29), H-9→L+7(3.01), H-7→L(2.55)
	14	3.6753	H-6→L+1(82.09), H-6→L+3(3.94), H-3→L+1(3.2)
	15	3.7561	H-13→L+3(2.22), H-10→L+1(33.38), H-10→L+3(9.88), H-1→L+3(4.44), H→L+1(10.98), H→L+3(17.99), H→L+5(5.84)
	16	3.767	H-15→L+2(2.31), H-11→L(32.23), H-11→L+2(9.57), H-5→L+2(8.98), H-2→L(11.11), H-2→L+2(13.52), H-2→L+4(5.72)
	17	3.8613	H-11→L+2(2.5), H-9→L+14(9.69), H-8→L+10(3.12), H-7→L+12(14.84), H-7→L+13(4.27), H-7→L+14(5.55), H-5→L(16.17), H-5→L+2(2.03), H-5→L+4(5.49), H-5→L+10(2.11), H-2→L(3.07), H-2→L+2(2.19)

Table S26. The singlet and triplet excited states transition configurations of cong-*R*-**1**-365nmUV dimer revealed by TD-DFT calculations. The matched excited states that contain the same orbital transition components of S_1 were highlighted in red.

	n-th	Energy (eV)	Transition configuration (%)
S_n	1	3.4837	H-5→L(68.54), H-3→L(27.01)
	2	3.5201	H-1→L+1(92.46), H→L+1(4.12)
T_n	1	2.7409	H-13→L+1(4.81), H-10→L+1(2.79), H-10→L+5(3.2), H-1→L+1(9.53), H→L+1(39.77), H→L+3(24.66)
	2	2.7459	H-15→L(7.11), H-11→L(2.18), H-11→L+4(4.02), H-5→L(24.87), H-5→L+2(5.64), H-3→L(24.26), H-3→L+2(18.44)
	3	3.0333	H-7→L+12(3.59), H-5→L(41.9), H-5→L+2(4.04), H-5→L+4(2.71), H-5→L+10(2.04), H-3→L(29.08)
	4	3.0522	H-2→L+15(2.64), H-1→L+1(61.94), H-1→L+3(3.23), H-1→L+5(2.9), H-1→L+11(3.53), H→L+1(8.73)
	5	3.1567	H-9→L(9.9), H-9→L+10(2.03), H-9→L+12(2.33), H-9→L+14(2.0), H-8→L(47.68), H-8→L+2(3.48), H-8→L+7(4.55), H-7→L(2.67), H-7→L+14(3.2), H-3→L(2.25), H-3→L+2(2.45)
	6	3.174	H-6→L+1(7.49), H-6→L+15(2.93), H-4→L+1(47.67), H-4→L+3(3.37), H-4→L+8(3.07), H-2→L+1(3.99), H-2→L+17(3.11), H→L+3(2.23)
	7	3.3658	H-13→L+1(12.01), H-12→L+1(3.78), H-12→L+8(4.63), H-12→L+9(4.68), H-10→L+1(10.26), H-10→L+3(8.59), H→L+3(14.9), H→L+5(4.31), H→L+8(3.84), H→L+9(2.82)
	8	3.3737	H-15→L(16.47), H-14→L+6(7.19), H-11→L(8.13), H-11→L+2(9.08), H-3→L+2(14.01), H-3→L+4(7.08), H-3→L+7(4.1)
	9	3.491	H-10→L+1(34.41), H-10→L+5(4.19), H-2→L+1(5.19), H-1→L+1(2.17), H→L+1(26.88), H→L+3(9.8)
	10	3.5019	H-11→L(16.66), H-11→L+4(2.34), H-7→L(48.29), H-5→L(5.99), H-3→L(8.4), H-3→L+2(3.28)
	11	3.5319	H-11→L(20.97), H-11→L+4(2.62), H-8→L(8.44), H-7→L(32.88), H-5→L(2.8), H-3→L(11.12), H-3→L+2(5.2)
	12	3.5605	H-4→L+1(11.46), H-2→L+1(72.24)
	13	3.6076	H-9→L(74.02), H-9→L+2(2.97), H-8→L(10.45), H-7→L(3.63)
	14	3.6447	H-6→L+1(75.72), H-6→L+3(2.86), H-4→L+1(6.51), H-2→L+1(4.66)
	15	3.7616	H-13→L+3(2.39), H-10→L+1(25.68), H-10→L+3(10.79), H-1→L+3(5.6), H→L+1(12.7), H→L+3(17.95), H→L+5(6.0)
	16	3.7702	H-15→L+2(2.68), H-11→L(24.58), H-11→L+2(10.39), H-5→L+2(13.53), H-3→L(12.86), H-3→L+2(10.16), H-3→L+4(5.59)
	17	3.844	H-11→L+2(3.21), H-9→L+14(9.4), H-8→L+10(3.56), H-8→L+14(4.17), H-7→L+12(18.88), H-7→L+14(3.09), H-5→L(15.48), H-5→L+4(5.66), H-5→L+10(2.36), H-3→L(4.01), H-3→L+2(3.32)

Table S27. The singlet and triplet excited states transition configurations of cong-*R*-**1**-395nmUV dimer revealed by TD-DFT calculations. The matched excited states that contain the same orbital transition components of S_1 were highlighted in red.

	n-th	Energy (eV)	Transition configuration (%)
S_n	1	3.4887	H-5→L(58.51), H-4→L(12.29), H-3→L(24.03)
	2	3.5258	H-1→L+1(92.01), H→L+1(4.13)
T_n	1	2.7372	H-13→L+1(5.55), H-10→L+1(2.59), H-10→L+5(3.05), H-1→L+1(8.97), H→L+1(41.45), H→L+3(24.25)
	2	2.7424	H-15→L(7.51), H-15→L+7(2.21), H-11→L+4(3.87), H-5→L(19.26), H-5→L+2(4.11), H-4→L(3.44), H-3→L(27.21), H-3→L+2(18.86)
	3	3.0362	H-7→L+12(3.1), H-5→L(37.0), H-5→L+2(3.38), H-5→L+4(2.64), H-4→L(7.79), H-3→L(26.21)
	4	3.0559	H-2→L+15(2.26), H-1→L+1(62.76), H-1→L+3(3.34), H-1→L+5(3.16), H-1→L+11(3.35), H→L+1(8.08)
	5	3.1721	H-9→L(27.99), H-9→L+10(3.35), H-8→L(31.07), H-8→L+2(2.71), H-8→L+7(5.08), H-8→L+12(2.94), H-7→L+14(2.92), H-3→L+2(2.19)
	6	3.1882	H-6→L+1(9.46), H-6→L+13(2.46), H-6→L+15(2.9), H-5→L+1(5.87), H-4→L+1(42.58), H-4→L+3(3.32), H-4→L+8(2.65), H-2→L+17(2.84), H→L+3(2.06)
	7	3.3784	H-13→L+1(13.52), H-12→L+8(5.52), H-12→L+9(5.77), H-10→L+1(8.79), H-10→L+3(8.11), H→L+3(15.91), H→L+5(4.14), H→L+8(3.7), H→L+9(3.42)
	8	3.3853	H-15→L(16.88), H-14→L+6(10.29), H-11→L(6.77), H-11→L+2(8.5), H-11→L+7(2.35), H-3→L+2(15.16), H-3→L+4(7.12), H-3→L+7(5.64)
	9	3.4993	H-11→L(6.84), H-7→L(74.09), H-3→L(4.28)
	10	3.5028	H-10→L+1(35.03), H-10→L+5(4.26), H-2→L+1(8.59), H→L+1(25.35), H→L+3(8.72)
	11	3.5377	H-14→L+6(2.73), H-11→L(32.35), H-11→L+4(4.17), H-8→L(3.31), H-7→L(11.11), H-5→L(5.77), H-3→L(16.07), H-3→L+2(7.43), H-3→L+7(2.56)
	12	3.5519	H-10→L+1(2.67), H-4→L+1(3.94), H-2→L+1(76.42), H-2→L+3(2.15), H→L+1(2.17)
	13	3.6058	H-9→L(49.75), H-8→L(36.06), H-7→L(2.01)
	14	3.6425	H-6→L+1(72.89), H-6→L+3(2.87), H-5→L+1(5.84), H-4→L+1(6.34), H-2→L+1(2.3)
	15	3.766	H-13→L+3(2.76), H-10→L+1(25.75), H-10→L+3(10.14), H-1→L+3(5.41), H→L+1(12.81), H→L+3(18.09), H→L+5(5.73)
	16	3.7739	H-15→L+2(2.71), H-11→L(24.32), H-11→L+2(9.29), H-5→L+2(10.57), H-3→L(13.87), H-3→L+2(10.56), H-3→L+4(5.65)
	17	3.8359	H-11→L+2(4.04), H-9→L+14(4.07), H-8→L+14(6.11), H-7→L+10(2.09), H-7→L+11(2.58), H-7→L+12(15.77), H-7→L+14(6.11), H-5→L(14.18), H-5→L+4(5.64), H-4→L(3.02), H-3→L(2.31), H-3→L+2(3.99)

References

1 C. Sun, J. S. Lu and S. N. Wang, *Org. Lett.*, 2011, **13**, 1226−1229.

2 O. V. Dolomanov, L. J. Bourhis, R. J. Gildea, J. A. K. Howard and H Puschmann, *J. Appl. Crystallogr.*, 2009, **42**, 339−341.

3 G. M. Sheldrick, *Acta Crystallogr., Sect. A: Found. Crystallogr.*, 2008, **64**, 112−122.

4 G. M. Sheldrick, *Acta Crystallogr., Sect. A: Found. Adv.*, 2015, **71**, 3−8.

5 A. R. Karim, A. Linden, K. K. Baldridge and J. S. Siegel, *Chem. Sci.*, 2010, **1**, 102−110.

6 R. Ahlrichs, *Phys. Chem. Chem. Phys.*, 2006, **8**, 3072−3077.

7 F. Neese, *Wiley Interdiscip. Rev.: Comput. Mol. Sci.*, 2012, **2**, 73−78.

8 W. Humphrey, A. Dalke and K. Schulten, *J. Mol. Graphics*, 1996, **14**, 33−38.

9 M. J. Frisch, G. W. Trucks, H. B. Schlegel, G. E. Scuseria, M. A. Robb, J. R. Cheeseman, G. Scalmani, V. Barone, B. Mennucci, G. A. Petersson, H. Nakatsuji, M.Caricato, X. Li, H. P. Hratchian, A. F. Izmaylov, J. Bloino, G. Zheng, J. L. Sonnenberg, M. Hada, M. Ehara, K. Toyota, R. Fukuda, J. Hasegawa, M. Ishida, T. Nakajima, Y. Honda, O. Kitao, H. Nakai, T. Vreven, J. A. Montgomery Jr., J. E. Peralta, F. Ogliaro, M. Bearpark, J. J. Heyd, E. Brothers, K. N. Kudin, V. N. Staroverov, T. Keith, R. Kobayashi, J. Normand, K. Raghavachari, A. Rendell, J. C. Burant, S. S. Iyengar, J. Tomasi, M. Cossi, N. Rega, J. M. Millam, M. Klene, J. E. Knox, J. B. Cross, V. Bakken, C. Adamo, J. Jaramillo, R. Gomperts, R. E. Stratmann, O. Yazyev, A. J. Austin, R. Cammi, C. Pomelli, J. W. Ochterski, R. L. Martin, K. Morokuma, V. G. Zakrzewski, G. A. Voth, P. Salvador, J. J. Dannenberg, S. Dapprich, A. D. Daniels, O. Farkas, J. B. Foresman, J. V. Ortiz, J. Cioslowski and D. J. Fox, Gaussian 09, D.01 Gaussian, Inc., Wallingford CT, 2013.